


Fall 2012

Oscillator-based neuronal modeling for seizure progression investigation and seizure control strategy

Wu Chen

Follow this and additional works at: <https://digitalcommons.latech.edu/dissertations>

 Part of the [Biomedical Engineering and Bioengineering Commons](#), and the [Nanoscience and Nanotechnology Commons](#)

**OSCILLATOR-BASED NEURONAL MODELING FOR
SEIZURE PROGRESSION INVESTIGATION
AND SEIZURE CONTROL STRATEGY**

by

Wu Chen, B.S.

A Dissertation Presented in Partial Fulfillment
Of the Requirements of the Degree
Doctor of Philosophy

COLLEGE OF ENGINEERING AND SCIENCE
LOUISIANA TECH UNIVERSITY

November 2012

UMI Number: 3534294

All rights reserved

INFORMATION TO ALL USERS

The quality of this reproduction is dependent upon the quality of the copy submitted.

In the unlikely event that the author did not send a complete manuscript and there are missing pages, these will be noted. Also, if material had to be removed, a note will indicate the deletion.



UMI 3534294

Published by ProQuest LLC 2012. Copyright in the Dissertation held by the Author.

Microform Edition © ProQuest LLC.

All rights reserved. This work is protected against unauthorized copying under Title 17, United States Code.



ProQuest LLC
789 East Eisenhower Parkway
P.O. Box 1346
Ann Arbor, MI 48106-1346

LOUISIANA TECH UNIVERSITY
THE GRADUATE SCHOOL

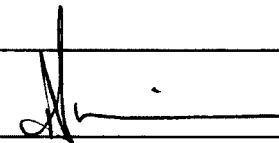
JULY 24, 2012

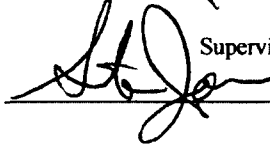
Date

We hereby recommend that the dissertation prepared under our supervision by
Wu Chen, B.S.

entitled **Oscillator-Based Neuronal Modeling For**
Seizure Progression Investigation
And Seizure Control Strategy

be accepted in partial fulfillment of the requirements for the Degree of
Doctor of Philosophy in Biomedical Engineering

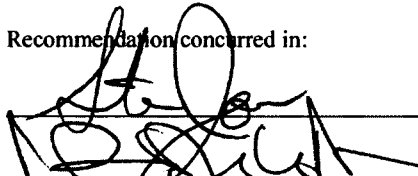


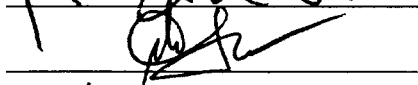
Supervisor of Dissertation Research



Head of Department

Department

Recommendation concurred in:








Advisory Committee

Approved:




Director of Graduate Studies

Approved:



Dean of the Graduate School



Dean of the College

ABSTRACT

The coupled oscillator model has previously been used for the simulation of neuronal activities in *in vitro* rat hippocampal slice seizure data and the evaluation of seizure suppression algorithms. Each model unit can be described as either an oscillator which can generate action potential spike trains without inputs, or a threshold-based unit. With the change of only one parameter, each unit can either be an oscillator or a threshold-based spiking unit. This would eliminate the need for a new set of equations for each type of unit. Previous analysis has suggested that long kernel duration and imbalance of inhibitory feedback can cause the system to intermittently transition into and out of ictal activities. The state transitions of seizure-like events were investigated here; specifically, how the system excitability may change when the system undergoes transitions in the preictal and postictal processes. Analysis showed that the area of the excitation kernel is positively correlated with the mean firing rate of the ictal activity. The kernel duration is also correlated to the amount of ictal activity. The transition into ictal activity involved the escape from the saddle point foci in the state space trajectory identified by using Newton's method.

The ability to accurately anticipate and suppress seizures is an important endeavor that has tremendous impact on improving the quality of lives for epileptic patients. The stimulation studies have suggested that an electrical stimulation strategy that uses the intrinsic high complexity dynamics of the biological system may be more effective in

reducing the duration of seizure-like activities in the computer model. In this research, we evaluate this strategy on an *in vitro* rat hippocampal slice magnesium-free model. Simulated postictal field potential data generated by an oscillator-based hippocampal network model was applied to the CA1 region of the rat hippocampal slices through a multi-electrode array (MEA) system. It was found to suppress and delay the onset of future seizures temporarily. The average inter-seizure time was found to be significantly prolonged after postictal stimulation when compared to the negative control trials and bipolar square wave signals. The result suggests that neural signal-based stimulation related to resetting may be suitable for seizure control in the clinical environment.

APPROVAL FOR SCHOLARLY DISSEMINATION

The author grants to the Prescott Memorial Library of Louisiana Tech University the right to reproduce, by appropriate methods, upon request, any or all portions of this Dissertation. It is understood that "proper request" consists of the agreement, on the part of the requesting party, that said reproduction is for his personal use and that subsequent reproduction will not occur without written approval of the author of this Dissertation. Further, any portions of the Dissertation used in books, papers, and other works must be appropriately referenced to this Dissertation.

Finally, the author of this Dissertation reserves the right to publish freely, in the literature, at any time, any or all portions of this Dissertation.

Author 

Date 2012. 10. 17

TABLE OF CONTENTS

ABSTRACT.....	iii
LIST OF TABLES.....	viii
LIST OF FIGURES	ix
ACKNOWLEDGMENTS	xii
CHAPTER 1 INTRODUCTION	1
1.1 General Overview	1
1.2 Research Objective	2
1.3 Dissertation Organization	5
CHAPTER 2 BACKGROUND	7
2.1 Seizure Characteristics.....	7
2.1.1 Epilepsy and Seizure Disease	7
2.1.2 Seizure on Brain Hippocampal Anatomy	8
2.1.3 Current Seizure Therapy	9
2.2 <i>In Vitro</i> Seizure Models.....	10
2.3 Computational Models on Single Neuron and Neuronal Network.....	11
2.3.1 Neural Modeling Description	11
2.3.2 Conductance-Based Model	12
2.3.3 Integrate-and-Fire Model	16
2.3.4 Mapped Clock Oscillators (MCO) Model	22
2.4 Seizure Stimulation Methods.....	30

CHAPTER 3 METHODS	33
3.1 <i>In Vitro</i> Data Acquisition.....	33
3.2 Model Description	35
3.3 Statistical Comparison	40
3.4 <i>In Vitro</i> Hippocampal Slice Seizure Model.....	42
3.5 Model Cognitive Rhythm Generator Model.....	42
3.6 Field Stimulation.....	43
CHAPTER 4 RESULTS	46
4.1 Threshold-Based Oscillation Model Output.....	46
4.2 Low-Magnesium Seizure-Like Activity Simulation.....	50
4.3 Network State Space Analysis.....	53
4.4 Negative Control Experiment	56
4.5 Suppression of Seizure-Like Events.....	57
CHAPTER 5 DISCUSSION.....	59
5.1 Slice Seizure Modeling.....	59
5.2 Slice Seizure-like Activity Control.....	63
CHAPTER 6 CONCLUSIONS AND FUTURE WORK.....	69
APPENDIX A THE MATLAB SOURCE CODE OF CRG MODEL	72
A.1 Main Function Code	73
A.2 The Derivative Function of CRG Model	79
A.3 Threshold Detection Function of CRG Model	83
A.4 Gaussian Function and R Function of CRG Model	85
A.5 Matching Function for Model Outputs and Biological Data	86
APPENDIX B THE R PROGRAM CODE OF STATISTICAL ANALYSIS.....	92
BIBLIOGRAPHY.....	98

LIST OF TABLES

Table 3-1: Model parameter symbols, explanations, and values used in the simulations	39
Table 4-1: A slice-by-slice summary of FF statistical comparison between the <i>in vitro</i> hippocampal slice data and the CRG model output is shown. The model was able to match each seizure state with $P > 0.05$. The relative system excitability measure (k/β) is at its highest value during the ictal state	52

LIST OF FIGURES

Figure 1-1:	Schematic of Research Plan: Incorporate the biological data into the computational model and use the negative control strategy to test the hypothesis.....	3
Figure 2-1:	Schematic representation of hippocampal anatomy.....	9
Figure 2-2:	Electrical Circuit for HH model description (Gerstner & Kistler, 2002)...	12
Figure 2-3:	FitzHugh-Nagumo model illustration (Izhikevich, 2007).....	14
Figure 2-4:	FitzHugh-Nagumo model run without external stimulation (FitzHugh, 1961)	15
Figure 2-5:	FitzHugh-Nagumo model runs with the stimulation (FitzHugh, 1961).....	16
Figure 2-6:	The illustration of InF model (Gerstner & Kistler, 2002).....	18
Figure 2-7:	The InF model output over time (Gerstner & Kistler, 2002).....	18
Figure 2-8:	Dynamics of the Izhikevich model (Izhikevich, 2003).....	20
Figure 2-9:	Various patterns generated by the different parameter combinations (Izhikevich, 2003)	21
Figure 2-10:	A schematic representation of a two-cell oscillator model is shown. Four biologically relevant coupling portals are proposed: electric field, synapse, extrasynaptic, and gap junction. The inputs to each oscillator are connected through portals with effective coupling weights.....	23
Figure 2-11:	The intrinsic waveform the MCO model (Zalay & Bardakjian, 2008).....	26
Figure 2-12:	The flow map of the MCO model (Zalay & Bardakjian, 2008)	27
Figure 2-13:	The model output of the Labile clock (Zalay & Bardakjian, 2008).....	29
Figure 2-14:	The model output of the hourglass (Zalay & Bardakjian, 2008)	30
Figure 2-15:	EEG seizure control feedback system using the responsive stimulation (Colpan et al., 2007).....	31

Figure 3-1:	A schematic illustration of a transverse hippocampal slice (Freund & Buzsaki, 1996). Whole-cell patch-clamp recordings of pyramidal neurons were conducted in the cell body layer of the CA1 hippocampal subfield.....	35
Figure 3-2:	A four-unit CRG model consisting of two excitatory units (one and two) and two inhibitory units (three and four) along with the coupling coefficients are illustrated. Units Three and Four are also threshold-based units.....	38
Figure 3-3:	Simulated field potential generated using the modified CRG model, illustrating spontaneous generation and termination of SLEs.....	43
Figure 3-4:	Oscillator-based postictal field data was repeated to create the stimulation signals that are 15-seconds in length.....	45
Figure 4-1:	The mean firing rate and the mean duration of the LPR mode, were evaluated as a function of β , k , X , as well as the excitation ratio of k/β . All of the analyses were performed on the model output signal from Unit One. (A) The overall percentage of time that a system stays in the LPR mode is most correlated to the kernel duration ($p < 0.05$). (B) The modulation gain affects the average duration of the LPR mode negatively ($p < 0.05$). (C) The modulation gain, excitation ratio, and DC excitation level are positively correlated to the mean firing rate within the LPR mode (Pearson correlation coefficient: $r = 0.9721, 0.9810$ and 0.9791 , respectively; $p < 0.05, p < 0.05$ and $p < < 0.001$, respectively). The mean firing rate is also found to be inversely proportional to the kernel duration	48
Figure 4-2:	The model outputs (from Unit One) are illustrated for different combinations of β , k , and X . Using (A) as the control, the parameters were changed one at a time. The parameters β and k both control the firing rates. (B) The mean firing rate decreases with an increasing β , while a larger k leads to a higher firing rate (C). (D) The parameter X mainly affects the firing pattern switching, and can also slightly increase the mean firing rate.	49
Figure 4-3:	Matching the biological data with the CRG model output during (A) preictal, (B) ictal, and (C) postictal activities. The time varying ISI plot for each condition is also shown. The major differences between the different parameter combinations are related to the location of the periodic orbits (mean firing rate), and the duration in which the system stays in the LPR mode	51

- Figure 4-4: An illustrative example of the best-fit simulated CRG matched with the biological data is shown. (A) The state-space trajectories (u_{11} , u_{31} , u_{41}) for different β values in the simulation are shown, demonstrating that the onset of SLE can be visualized as the departure from the saddle point foci in interictal dynamics. The ictal dynamics exhibits a quasi-periodic trajectory. (B) The simulated signals (from Unit One of the model) along with the *in vitro* data (from Slice One) at different SLE states are also illustrated to show the similarity between the model output and the *in vitro* patch-clamp recordings. However, the similarity of the amplitude and the spike distribution still can be improved by adjusting the model parameters..... 55
- Figure 4-5: Sample field measurement from the negative control experiment showing repeated SLEs at approximately 8.30 ± 2.23 times every ten minutes..... 56
- Figure 4-6: The effect of postictal stimulation (PS) on Mg-free *in vitro* hippocampal slice seizure model is shown. The seizure-like events are denoted as SLE. After stimulation (PS), interictal spiking events (*) were generated, leading to delayed or prolonged inter-seizure time 58
- Figure 4-7: Ranksum statistics was performed on the negative control (NC) and postictal stimulation (PS) trials, showing that PS stimulation can prolong the inter-seizure time ($p < 0.002$). 58
- Figure 6-1: Sketch of the feedback control system for seizure suppression test 71

ACKNOWLEDGMENTS

I am grateful to the people who have helped me to fulfill this dissertation. I wish to express my sincere gratitude and appreciation to my advisor, Dr. Alan Chiu, for his generous advice and guidance with great patience. It is my honor to be his student. Without his guidance and advice, this dissertation could not have been completed. I would like to thank Dr. Mark DeCoster for his support and for his neuroscience class. I would also like to extend thanks to Dr. Steven Jones for his help and his physiological modeling class and to Dr. Dexter Cahoy for his research cooperation and his time series class. I would like to thank to Dr. Teresa Murray for her kind help in my dissertation. I thank all of the professors above for their kindness of serving as advisory committee members. Sincere acknowledgement is also extended to Dr. James Spaulding for his patience in managing the electrophysiology lab. I express special appreciation to Dr. Jeffrey Tasker and Dr. Shi Di of Tulane University for their intracellular recording technique training.

My heart is full of thanks to my parents, my father Yongsen Chen, my mother Yuanyuan Jiang and my girlfriend Zhiying Jiang for their generous support and providing me with comfortable conditions for living and studying. Finally, I want to express my appreciation to all my friends. This dissertation is dedicated to all of those named above.

CHAPTER 1

INTRODUCTION

1.1 General Overview

Epilepsy is a common neurological disorder affecting up to 1% of the world's population and may be caused by head injuries, high fever, low blood sugar level, poisoning, drug overdose, infection, or other genetic factors (Buck et al., 1997; Merlin, 2009; Cockerell, 1996; Netoff et al., 2004; Kamali et al., 2004). Seizures are transient interruptions of brain function caused by abnormal temporal and spatial coherent firing of a neuronal population, lasting from a few seconds to a few minutes (Chiu et al., 2006a). Approximately 30% of all the patients suffering from epilepsy are intractable towards antiepileptic drug (AED) treatments (Schmidt & Löscher, 2005). Non-responders to AED may be treated with surgical resections. Surgeries can be performed to resect areas of the brain where seizures originate, or to create a series of incisions to prevent seizures from spreading to other parts of the brain. For those not eligible for surgeries, the ability to anticipate seizures and provide potential treatments in the form of electrical stimulation is at the forefront of epilepsy research (Fisher et al., 2010; Lehnertz et al., 1998; Morrell, 2011; Stacey & Litt, 2008). The development of such a system could greatly enhance the quality of life of patients, providing them with early warnings of impending seizures, and automatic interventional therapy for the prevention of seizure episodes.

A typical seizure event is indicated by the occurrence of low complexity, possibly rhythmic paroxysmal (LPR) electrical discharges called the ictal activity (Babloyantz & Destexhe, 1986; Lehnertz et al., 1998; Nair et al., 2009). High complexity is possibly chaotic (HPC) electrical brain activities that occur between the ictal events are the interictal regions. Multiple preictal states may exist between the interictal and ictal activities, which could potentially be used to develop seizure anticipation algorithms and may require different stimulation techniques depending on their proximities to the ictal onsets (Chiu et al., 2011; Colic et al., 2011).

The motivation of my dissertation is to improve upon previous research on seizure modeling and seizure stimulation which can be useful for current epilepsy therapy. In this case, biological signals from rat hippocampal brain slices with seizure-like activity were obtained and used to provide parameter values for a modified computational seizure model. The computational model was then used to identify firing patterns that were used to mitigate seizure activity in rat brain slices.

1.2 Research Objective

The brain signal generated during a seizure is different from that generated under normal conditions, so databases of electrical signals for both seizure and normal activity were acquired. After that a modified seizure model was created based on these electrophysiological signals, and then a control method for seizure suppression was developed based on the computational model output (Figure 1-1).

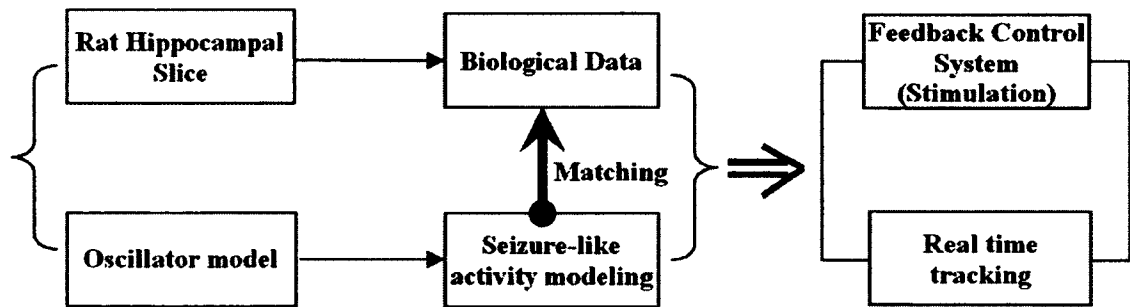


Figure 1-1: Schematic of Research Plan: Incorporate the biological data into the computational model and use the negative control strategy to test the hypothesis.

One goal of this research was to quantify the model parameters related to the network excitability during transitional dynamics between interictal and ictal activities. The kernel duration and amplitude were evaluated as the electrical activity in rat hippocampal brain slices (*in vitro* model) underwent different stages of preictal activities, as well as the return to interictal activity through the postictal process.

Several computational models were used and modified in this work. First, a modification was made to the Cognitive Rhythm Generator (CRG, Zalay & Bardakjian, 2009; Zalay et al., 2010) of seizure like activity (SLE). This model is robust and versatile because each model unit can become either an endogenous oscillator or a threshold-based spiking unit by adjusting a single model function variable. This is relevant to SLE transitions, providing a variant of the labile CRG previously proposed by Zalay and Bardakjian (2009). The probability distributions of the self-organized criticality property from human epilepsy patients have been reported and can be expressed as integrate-and-fire oscillator networks (Worrell et al., 2002), which may also be an emergent property of the coupled oscillators. One proposed physiological mechanism of epileptogenesis involves a gradual transformation from a normal threshold-based to a hyperexcitable state, which may involve sprouting of axonal collaterals leading to reverberating, or self-

reinforcing oscillatory circuits (Bromfield et al., 2006). This transition may be easily captured and the current model can provide another simulation platform for the evaluation of future stimulation protocols on spontaneous as well as evoked seizures. Second, a modified Kolmogorov-Smirnov-based statistical test (Fasano & Franceschini, 1987) was used to compare the dynamics of the biological data at different stages of SLEs and the simulated system outputs. Third, the reconstructed state space distributions of the *in vitro* experimental data undergoing SLE progression were compared with the simulated CRG network outputs at different system excitation levels on a slice-by-slice basis. This was necessary because a great deal of subject-to-subject spatial differences exist, as well as temporal variability, in the manifestation of seizure activities.

The next goal of this work was to evaluate and develop feedback control strategies to suppress or reduce the occurrence of seizures based on the improved computational model described above. Seizure anticipation algorithms (Zalay et al., 2010) in conjunction with responsive stimulation feedback control strategies (Colic et al., 2011; Wagenaar et al., 2005) for the suppression of seizures has been in the forefront of seizure research for many years. The mechanism of this kind of feedback is to maintain the normal activity of the neuronal networks when state transitions into seizures are detected. Many kinds of stimulation strategies have been proposed and tested, such as controlled pulse stimulation (Albensi et al., 2008) and high-frequency stimulation (Su et al., 2008). Most recently, the use of the high complexity dynamics of the biological interictal data as a responsive stimulator has shown great promise in a computer simulation study (Colic et al., 2011).

In conclusion, the objectives of this dissertation (Figure 1-1) are: (1) Improve and validate our computer simulation model based on the signals recorded from the rat brain slice: Task #1: Record the neuronal seizure-like activities using a whole-cell patch-clamp technique from the single neuron on the CA1 region of the rat's hippocampus; Task #2: Model a four-neuron network under different seizure conditions; Task #3: Carry out data analysis/validation using experimental data. (2) Design and validate a computational model based stimulation method to control seizure-like activities: Task #1: Design the stimuli from our seizure model outputs; Task #2: Apply our seizure control method to the hippocampal slice and record the output signal; Task #3: Evaluate the validity of the seizure stimulation results.

1.3 Dissertation Organization

Chapter One gives a general description of the research objectives in this dissertation.

Chapter Two introduces the main literature regarding the seizure characteristics in the rat hippocampal slice, particular models that represent the neuronal activities as well as previous works on the seizure control methods.

Chapter Three describes all the methods used in this dissertation including *in vitro* data acquisition, *in vitro* slice seizure model, the computational seizure model, seizure stimulation tools, and statistical analysis. They were applied to accomplish the tasks of seizure activities modeling and seizure-like event (SLE) stimulation. The statistical analysis helps to test the significance.

Chapter Four describes how the cognitive rhythm generator model was used to obtain various patterns of seizure-like activities under different conditions. The seizure

model output is matched to the data collected from in vitro slice seizure data. Statistical significance was defined as $p \leq 0.05$ using students' t-tests (two-tailed, two-sample with equal variance). Results from Sections 4.1-4.3 have been published in *Journal of Network: Computation in Neural Systems*. Results from Section 4.4-4.5 will appear as a juried conference paper in *IEEE EMBS Annual International Conference Proceedings 2012*.

Chapter Five discusses the computational model in detail and points out the advantage and disadvantage of this modified GRG SLE model. It also discusses the limitation of the seizure control strategy and the potential significance for seizure cure therapy.

Finally, Chapter Six summarizes the dissertation research and suggests future research.

CHAPTER 2

BACKGROUND

Chapter Two introduces the main literature regarding the seizure characteristics in the rat hippocampal slice, particular models that represent the neuronal activities, and previous work on the seizure control methods.

2.1 Seizure Characteristics

2.1.1 Epilepsy and Seizure Disease

Brain diseases affect brain control function which controls memory, learning, speech, and movement. Epilepsy is one of the most common mental diseases. It happens to 1 person in every 200 and can affect people of any age, race and sex from any walk of life. Seizure is a result of the disruption of brain activity in a brief time, which can be characterized by high frequency action potentials that last from seconds to minutes. Such disruptions occur for a variety of reasons, not all of which can be identified. Some of the reasons are brain damage, scarring, chemical or hormonal imbalance, and tumors (Buck et al., 1997; Merlin, 2009; Cockerell, 1996; Netoff et al., 2004; Kamali et al., 2004). Seizures can affect muscle movements, sensations, behaviors, emotions, consciousness, or a combination of these factors. Epilepsy is one of the most widely studied diseases with research areas that include epileptogenesis, nonlinear network dynamics, electrographical signal feature extraction, seizure anticipation and feedback control.

2.1.2 Seizure on Brain Hippocampal Anatomy

When a seizure occurs in the region of the brain that involves memory or learning, rather than regions which can be removed without serious effect to daily life, doctors cannot surgically ablate the brain tissue that causes the seizure. Thus, to suppress seizures in this region, recent research has focused on methods to electrically control brain activity in the hippocampus (Figure 2-1) which is a large structure related to human learning and memory in the subcortical region (Berger et al., 2005). Seizures can affect the synaptic current, neurotransmitter release, and receptor function (Avoli, 2007). So far as we know the hippocampus is responsible for long-term memory (Brivanlou et al., 2004; Yeckel et al., 1999). The basic hippocampal circuit (Figure 1-1) begins at the dentate gyrus (DG) and goes through a series of Cornu Ammonis (CA) areas from CA3 to CA1 pathway (Figure 2-1) (Brijesh & Ravindran, 2007). The CA areas have numerous types of neurons, such as pyramidal neurons and interneurons (Brivanlou et al., 2004). This signal pathway is so called the perforant path which is a suspected seizure propagation (Levy et al., 1998).

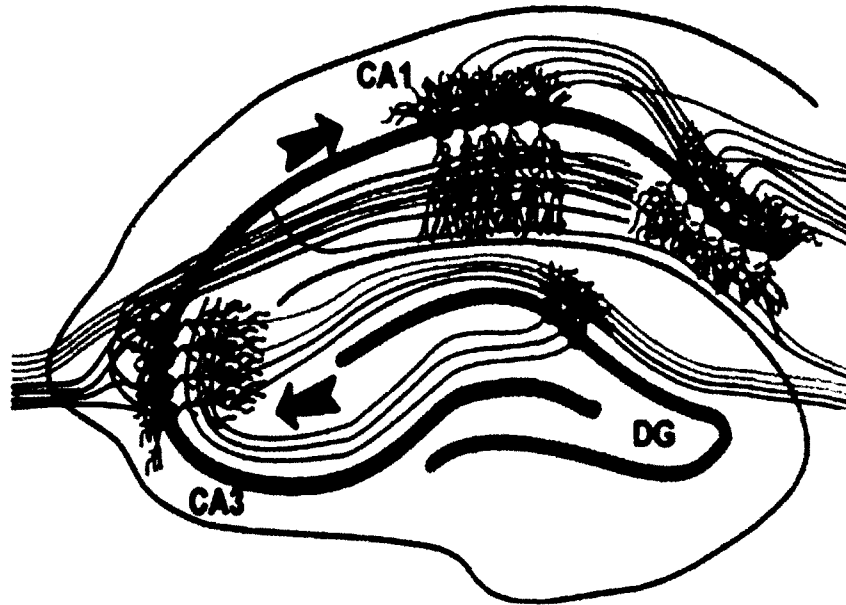


Figure 2-1: Schematic representation of hippocampal anatomy.

2.1.3 Current Seizure Therapy

Approximately 30% of all the patients suffering from epilepsy have seizures that are intractable towards antiepileptic drug (AED) treatments (Schmidt & Löscher, 2005). Non-responders to AED may be treated with surgical resections. Surgeries can be performed to resect areas of the brain where seizures originate, or to create a series of incisions to prevent seizures from spreading to other parts of the brain. For those not eligible for surgeries, the ability to anticipate seizures and provide potential treatments, in the form of electrical stimulation, is at the forefront of epilepsy research (Fisher et al., 2010; Lehnertz et al., 1998; Morrell, 2011; Stacey & Litt, 2008). The development of such a system could greatly enhance the quality of life of patients, providing them with early warnings of impending seizures, and automatic interventional therapy for the prevention or mitigation of seizure episodes.

2.2 *In Vitro* Seizure Models

Seizure in the rat hippocampal brain slices is characterized by hyper-exciting activity and synchronization of neuron firing. The pattern of this seizure-like activity has high frequency regular oscillation during the ictal period. It can be either induced by various chemical solutions or generated using different electrical stimulations. The neurons enter a high frequency, bursting state when these methods were applied. For chemical induction of SLE, the concentrations of specific ions are changed, such as raising K^+ , and/or lowering Mg^{2+} or Ca^{2+} (Traynelis & Dingledine, 1988; Walther et al., 1986; Albrecht et al., 1989). In contrast, the electrical seizure generating methods may cause serious damage to the cell so that the seizure activity is unable to regenerate ictal firing.

The most common method to obtain seizure-like activity in an *in vitro* animal slice model uses high K^+ /low Mg^{2+} . It provides a means to investigate the electrophysiological mechanisms and the transition between seizure (ictal) and inter seizure (interictal) periods. The concentrations of K^+ and Mg^{2+} in the artificial solution are around 3-5 mM and 0.5-0 mM, respectively. By varying the concentrations of K^+ and Mg^{2+} in the artificial cerebral spinal fluid, the brain slice can be used to obtain data on normal and SLE neuronal firing patterns. One of the most important advantages is the reversible nature of this transition. This allows each slice to act as its own negative control.

However, the difference between actual seizures and *in vitro* models is still not clear. Most likely epileptic seizures in a living animal, including humans, are more complicated processes than those in a slice model. This must be taken into account when

stimulation methods are designed for humans. Yet, the rat hippocampal brain slice models are cost-effective and contain enough features to make them useful for academic research and translational medicine.

2.3 Computational Models on Single Neuron and Neuronal Network

2.3.1 Neural Modeling Description

Many computational models of the biological neural systems have been designed and focused on different aspects of the neural systems. They are modeled to describe and predict the long-term and short-term plasticity of the neural systems and its relation to learning and memory, from the individual neuron to the system level.

In 1952, Hodgkin and Huxley first delivered their circuit model of the ionic mechanisms (Hodgkin, Huxley, & Katz, 1952). Later, FitzHugh and Nagumo described their model which simplified the Hodgkin-Huxley model (FitzHugh, 1961; Nagumo et al., 1962). In 1981, Morris and Lecar combined the two models above to generate their model of calcium and potassium channels (Morris & Lecar, 1981). In the following years, several additional models were published. Kernel-based neural models (Chon et al., 1998) were one of these in which the properties of the neurons were assessed experimentally by applying a Poisson distributed pulse train of electrical impulses to the system and electrophysiologically recording the evoked output (Dorval & White, 2006; Wyckhuys et al., 2010). The relationship between the input pulse train and the subsequent response of the neuron is represented mathematically as the kernel functions.

However, such an approach does not account for the intrinsic oscillatory behavior in some subfields of the hippocampus which is responsible for memory consolidation. In addition, the kernel estimation is static in that it is not able to adapt over time to account

for possible changes in synaptic characteristics for long term application. To address such deficiencies, Berj L. Bardakjian et al. (2008) designed the mapped clock oscillators (MCO) model with tunable connectivity (Zalay et al., 2010). This model can be utilized or modified and contributed to this research in seizure modeling and seizure feedback control.

2.3.2 Conductance-Based Model

The Hodgkin-Huxley (HH) model of action potential (AP) generation and propagation is the single most successful quantitative model in neuroscience. The model represents the cornerstone of quantitative models of neuronal excitability. The heart of the model (Figure 2-2) is a description of the time- and voltage-dependent conductance for Na^+ and K^+ in terms of their gating properties. Gating properties can be the activation or inactivation variety which implies its amplitude is from 0 to 1. This amplitude increases with depolarization while the converse is true of inactivation. Kinetics of gating is represented either by the rate constants or the steady states (activation/inactivation) and the time constants (Hodgkin, Huxley, & Katz, 1952). Without any a priori assumptions about action potentials, the model generates APs of appropriate shape, threshold and refractory periods (both absolute and relative).

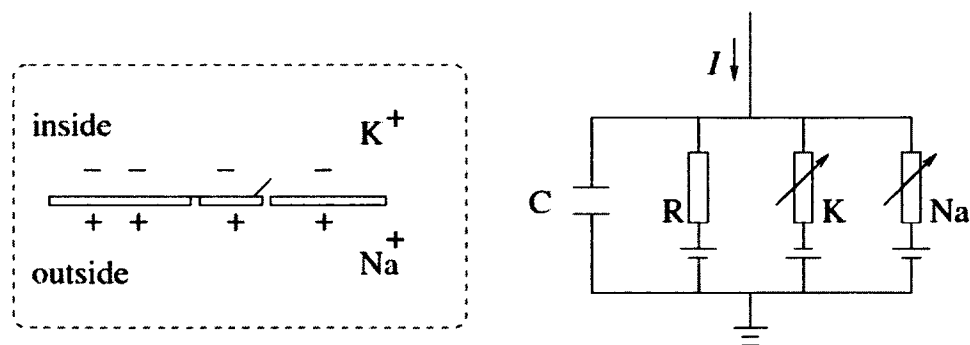


Figure 2-2: Electrical Circuit for HH model description (Gerstner & Kistler, 2002).

Consider each type of ionic channel as a distinct path of the current flow. The lipid bi-layer can be modeled as a capacitor (impermeable layer as separator for two sides of different electrical potential). Balance the current through each path using the Equations 2-1 and 2-2 (Hodgkin, Huxley, & Katz, 1952):

$$I_{inj}(t) = I_c(t) + \sum_k I_k(t), \quad \text{Eq. 2-1}$$

$$C \frac{dV_m}{dt} = - \sum_k I_k(t) + I_{inj}(t). \quad \text{Eq. 2-2}$$

Incorporating the sodium and potassium current after curve fitting of the conductance, we have (Hodgkin, Huxley, & Katz, 1952):

$$C \frac{dV_m}{dt} = -\bar{g}_{Na} m^3 h (V_m - E_{Na}) - \bar{g}_K n^4 (V_m - E_K) - \bar{g}_L (V_m - E_L) + I_{inj}. \quad \text{Eq. 2-3}$$

The transmembrane potential can be computed based on the Na-K pump dynamics. Since channels are highly selective, we can consider the movement of each ion as an independent path across the membrane. The dynamics of each channel is defined by the relationship between the driving force (electrical potential, or voltage) and the ionic movement (rate of change of ion concentration, or current). In general, $I = gV$, where I is the current [μA], V is voltage [mV] and g is conductance [mS]. As indicated by Figure 2-2, there are primarily four major current pathways that significantly affect the potential across the membrane: Sodium current, potassium current, leak current (related to ion pump and non-selective channels), and capacitive current.

Notice that the HH model is a fourth order system; when we consider a state space representation like this, it is difficult to visualize. Several reduction models have been proposed to collapse it onto two-dimension state space. The FitzHugh-Nagumo model is an example of such a reduction (FitzHugh, 1961; Nagumo et al., 1962) where

membrane potential is plotted against a recovery variable, w , in Figure 2-3 and the model equations are,

$$\dot{v} = v - v^3 - w + I_{ext}, \quad \text{Eq. 2-4}$$

$$r\dot{w} = v - a - bw, \quad \text{Eq. 2-5}$$

where v and w were dimensionless state variables representing the membrane potential and membrane recovery variable. The parameters (a , b and r) are dimensionless.

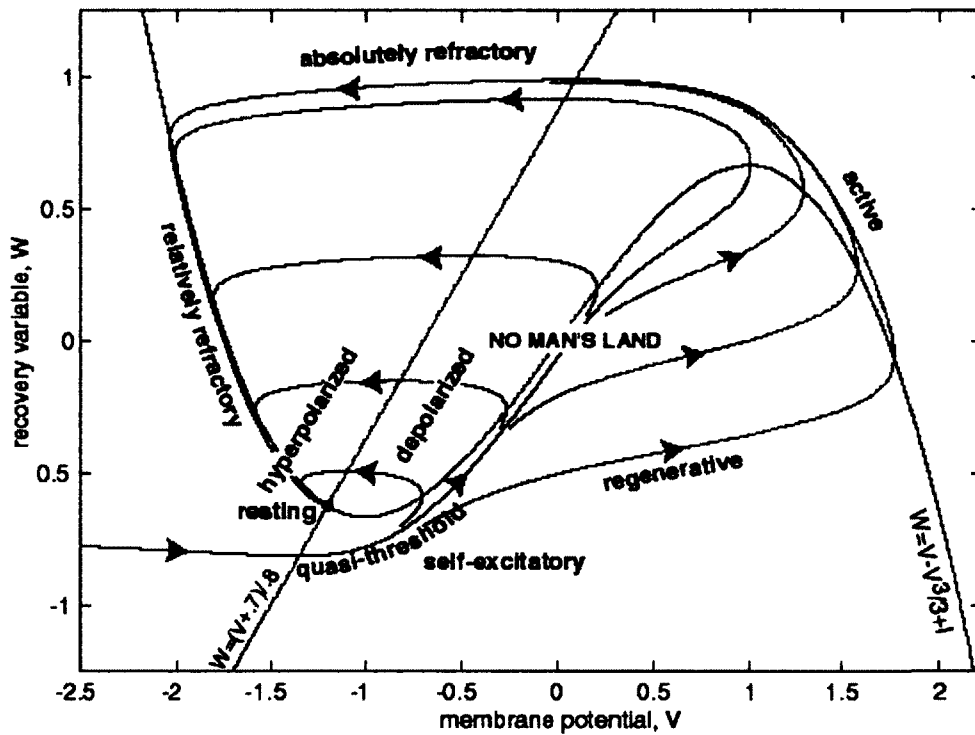


Figure 2-3: FitzHugh-Nagumo model illustration (Izhikevich, 2007).

An all-or-none spiking phenomenon in response to stimuli is illustrated above. However, excitation can lead to a block of oscillation. When I is weak or zero, there is not enough strength to drive the model to fire, so the model stays in a resting state. After increasing I input, the model enters the depolarization mode and starts firing. With external stimulation, the model can generate periodic bursting signal. However if I is further increased, the model turns into the refractory region. In this case, the firing action is stopped. The differences of the processes with stimulation and without stimulation are shown in Figures 2-4 and 2-5, respectively.

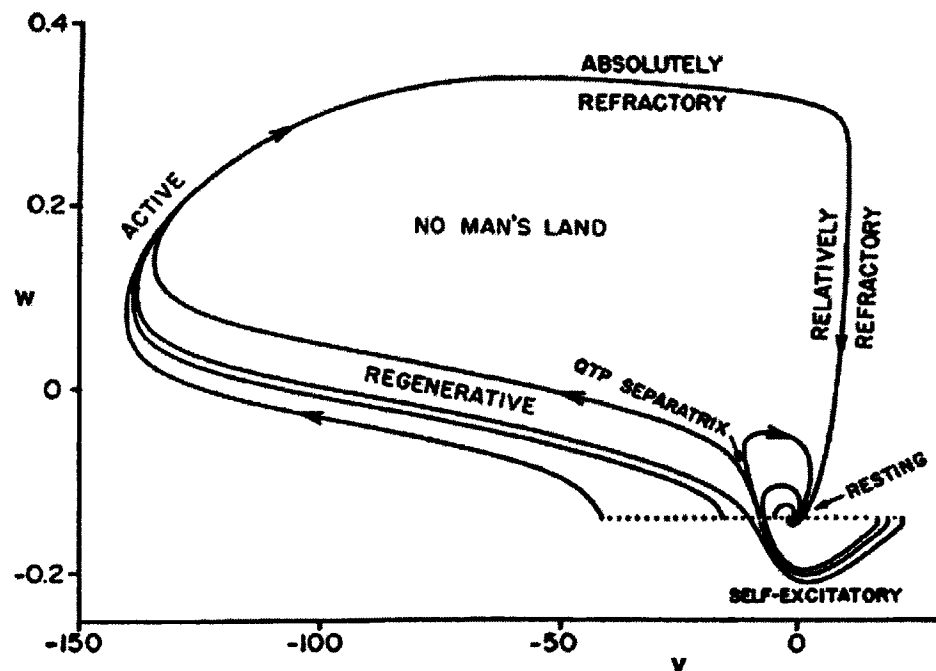


Figure 2-4: FitzHugh-Nagumo model run without external stimulation (FitzHugh, 1961).

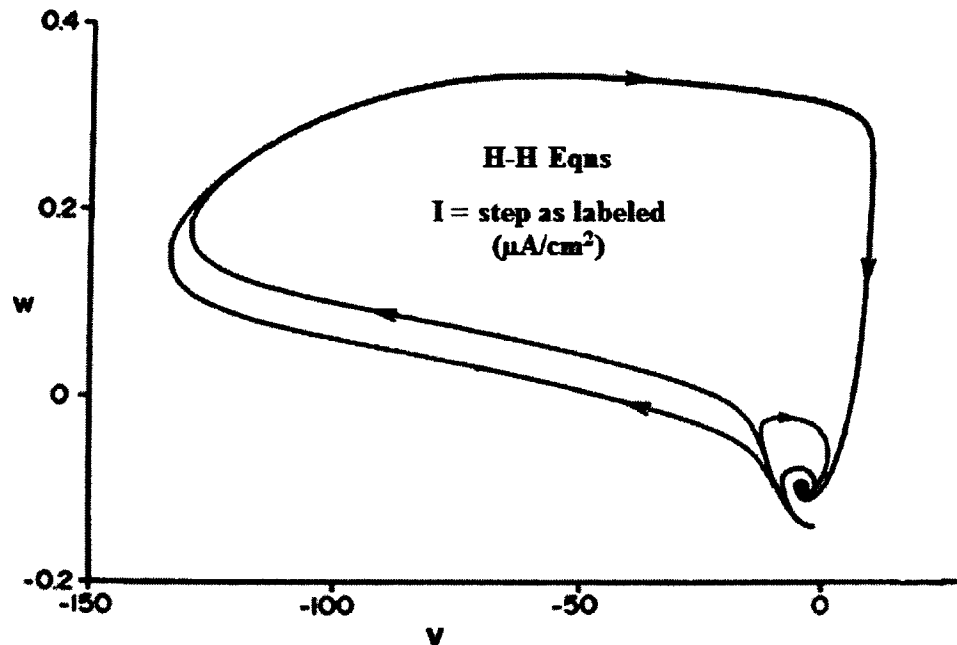


Figure 2-5: FitzHugh-Nagumo model runs with the stimulation (FitzHugh, 1961).

2.3.3 Integrate-and-Fire Model

The integrate-and-fire (InF) model (Figure 2-6) captures two key aspects of neuronal excitability: passive integrating response for (subthreshold) inputs and stereotypical waveform for excitation exceeding a particular amplitude (Lapicque, 2007).

In Figure 2-6, a neuron (or a model unit i) receives inputs from multiple neurons (j). After the convolution operation with the synaptic impulse response, the output is compared with a threshold. If the intermediate signal exceeds the threshold, a stereotypical waveform is created artificially. Different equations can be setup based on the HH model of the capacitor (C) and the resistors (R). When the voltage (u) reaches a threshold level (ϑ), a spike is created. This is an example of the leaky spiking model (Figure 2-7). When the voltage is smaller than the threshold, we have (Gerstner & Kistler, 2002; Lapicque, 2007)

$$C \frac{dV}{dt} = (g_L + g_{adapt})(V_L - V) + I_{ext}, \quad \text{Eq. 2-6}$$

$$\tau_{adapt} \frac{dg_{adapt}}{dt} = -g_{adapt}, \quad \text{Eq. 2-7}$$

where g_L is the leakage current and g_{adapt} is the sum of all ionic current. When the voltage is equal or larger than the threshold, we have (Gerstner & Kistler, 2002; Lapicque, 2007)

$$t \rightarrow \{Registered\ Spikes\} = \sum_k \delta(t - t_k), \quad \text{Eq. 2-8}$$

$$V([t, t + t_{ref}]) = V_{reset}, \quad \text{Eq. 2-9}$$

$$g_{adapt}(t) = g_{adapt} + G_{inc}. \quad \text{Eq. 2-10}$$

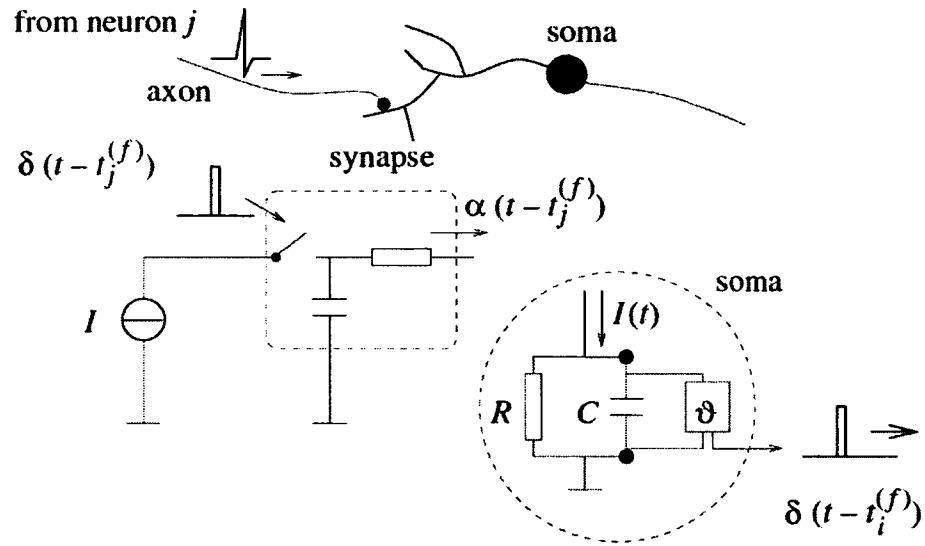


Figure 2-6: The illustration of InF model (Gerstner & Kistler, 2002).

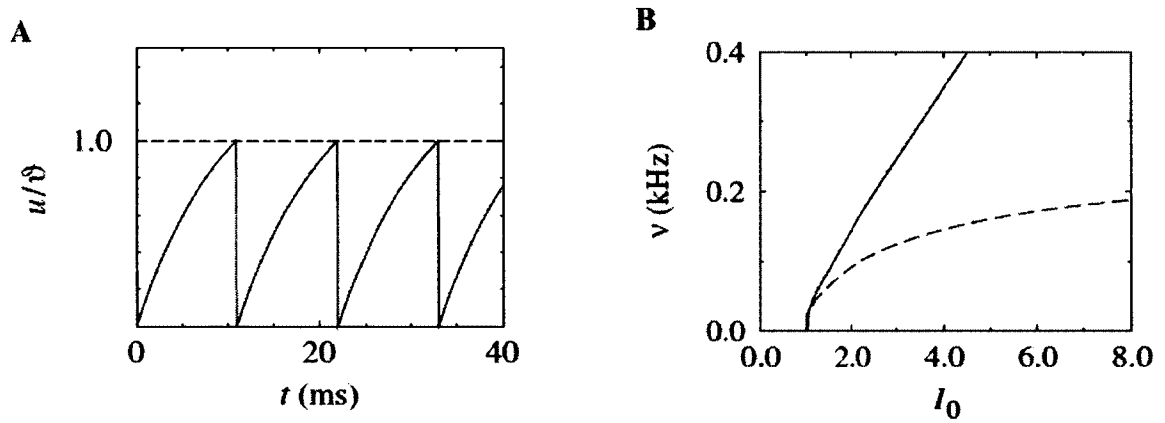


Figure 2-7: The InF model output over time (Gerstner & Kistler, 2002).

The major feature in this model is that the conductance can be adapted over time if a DC current is injected into the model so that the spike-to-spike interval will gradually increase. There is another example of an InF model that was published by Eugene M. Izhikevich (Figure 2-8) shown in Equations 2-11 and 2-12 (Izhikevich, 2003):

$$\dot{v} = 0.04v^2 + 5v + 140 - u + 1, \quad \text{Eq. 2-11}$$

$$\dot{u} = a(bv - u). \quad \text{Eq. 2-12}$$

If $v = 30$ mV, then $v = c$, $u = u + d$. Here, v and u are dimensionless state variables representing the membrane potential and membrane recovery variable, respectively (similar to modified HH), but the if-then statement is used to reset the voltage to below the threshold. The parameters (a , b , c and d) are dimensionless. They are obtained by curve fitting the spike initiation dynamics of the cortical neurons so that the membrane potential has mV scale and the time has ms scale. The definitions of the parameters are as follows:

- The parameter a describes the time scale of the recovery variable. The smaller the value, the slower the recovery. A typical value is $a = 0.02$.
- The parameter b describes the sensitivity of recovery to the subthreshold fluctuations of the membrane potential. A greater value of the coupling of v and u results in a higher probability of subthreshold oscillations and low-threshold spiking. A typical value for $b = 0.2$.
- The parameter c describes the after-spike reset value of the membrane potential caused by fast, high-threshold potassium conductance. A typical value for $c = -65$ mV.

- The parameter d describes the after-spike reset of the recovery variable caused by the slow, high-threshold sodium and potassium conductance. A typical value for $d = 2$.

Depending on the parameters selected, the different neuronal dynamics can be generated in Figure 2-9.

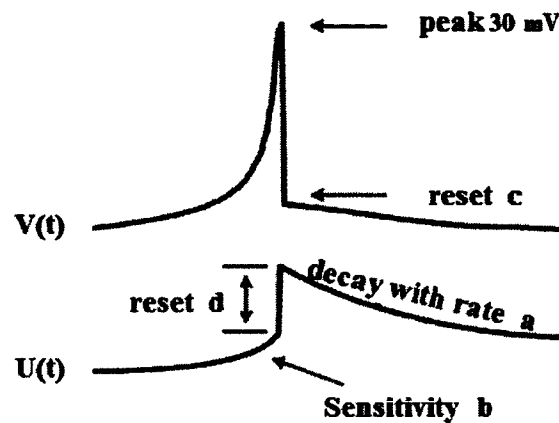


Figure 2-8: Dynamics of the Izhikevich model (Izhikevich, 2003).

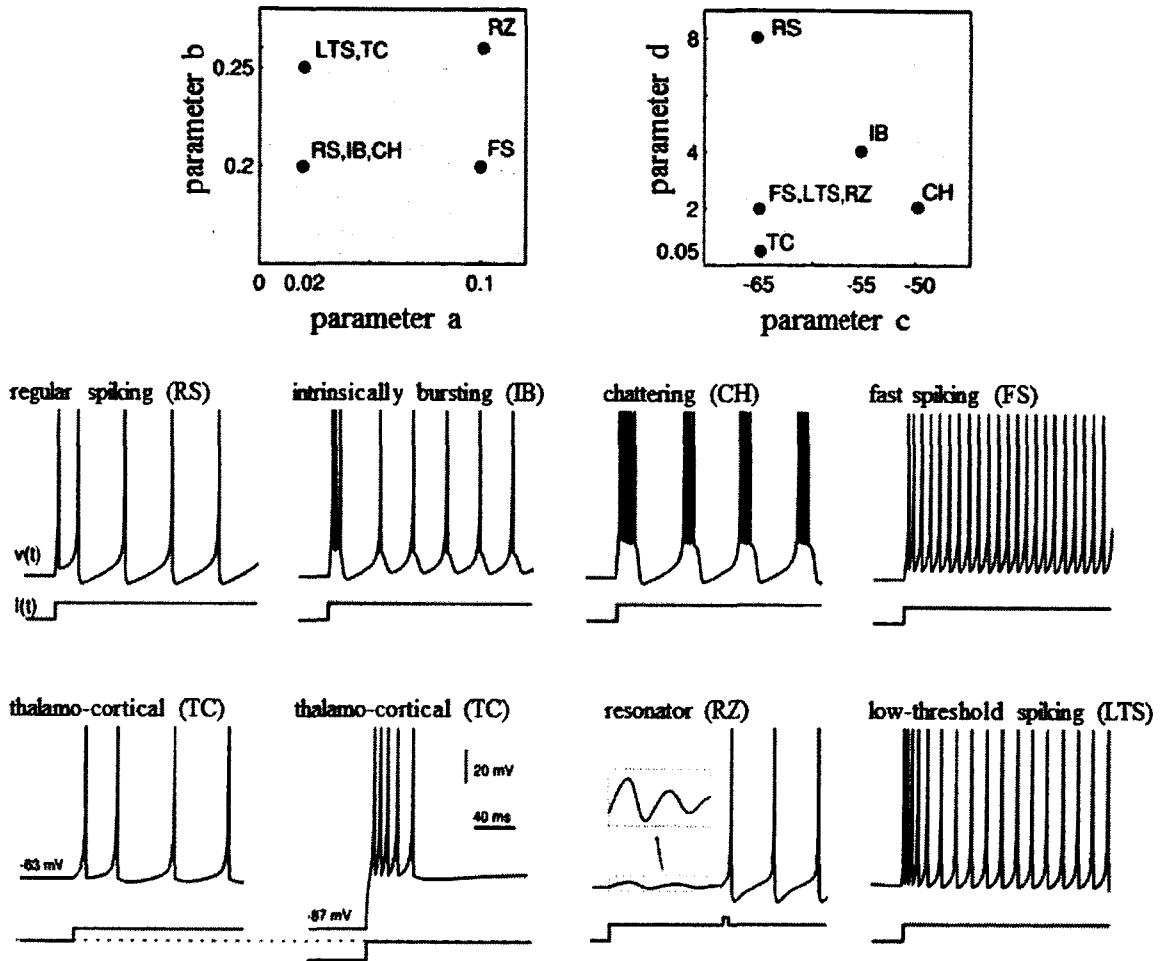


Figure 2-9: Various patterns generated by the different parameter combinations (Izhikevich, 2003).

2.3.4 Mapped Clock Oscillators (MCO) Model

The MCO model (Figure 2-10) is a multi-portal extension of the Winfree-type oscillator that includes not only the phase advance, but also amplitude variations (r) and a mapping function to relate the state variables (r, ϕ) to transmembrane voltage (y). Each oscillator unit is equipped with four input portals representing different modes of coupling (gap junction, electric field, chemical synapse, and extra-synaptic coupling) and stimulation (Bardakjian and Diamant, 1994; Zariffa et al., 2004). Entrainment properties of the coupled nonlinear oscillators are governed by the intrinsic unit properties and the coupling mechanisms. As a result, the model is able to adapt to different network configurations, neuronal classifications and stimulation protocols. It is innovative in two major aspects. First, it allows for the customization of intrinsic neural characteristics so the cellular mechanisms responsible for the generation of rhythmic neuronal firing can be studied. Second, the types and strengths of the neural model connections can be adjusted to accommodate for plasticity. For a potential biomimetic device, an oscillator model was chosen because it reflects some key dynamics of the hippocampal neurons. Three different types of model units have been proposed (Zalay & Bardakjian, 2008): Oscillators, Labile clock and Hourglass. Depending on the neuron type, an appropriate model unit is selected.

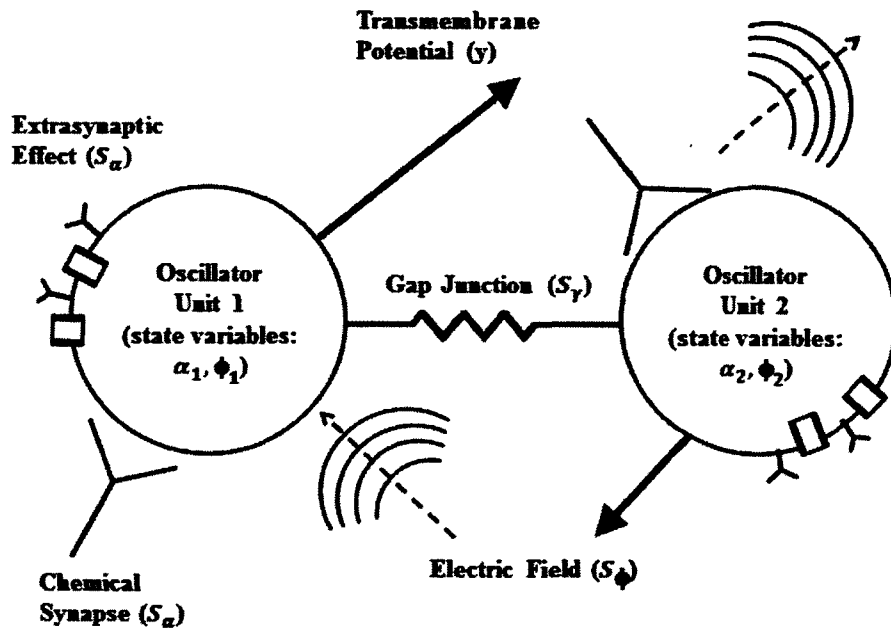


Figure 2-10: A schematic representation of a two-cell oscillator model is shown. Four biologically relevant coupling portals are proposed: electric field, synapse, extrasynaptic, and gap junction. The inputs to each oscillator are connected through portals with effective coupling weights.

For the oscillator, it is dependent on two variables, the amplitude and the phase. The most basic form of oscillation is a sine or cosine wave.

$$F_1(t) = \cos(2\pi ft), \quad \text{Eq. 2-13}$$

$$F_2(t) = \sin(2\pi ft). \quad \text{Eq. 2-14}$$

When F1 is plotted versus F2 on a 2-D plane, it produces a unit circle in Cartesian coordinates. When it is converted into polar coordinates, the result is a constant amplitude $r = 1$ and a phase advance at a constant rate of $2\pi f$. The MCO model is built based on this concept and can be expressed as follows (Zalay & Bardakjian, 2008):

$$\dot{r} = wr(1 + S_\alpha - r^2) + S_{\gamma 1} \sin(\varphi) + S_{\gamma 2} \cos(\varphi), \quad \text{Eq. 2-15}$$

$$\dot{\varphi} = w(1 + R(\varphi)S_\varphi) + \left(\frac{1}{r}\right)(S_{\gamma 1} \sin(\varphi) + S_{\gamma 2} \cos(\varphi)). \quad \text{Eq. 2-16}$$

Here r is the amplitude and φ is the phase information. Both of them are defined as a first order ordinary differential equation (ODE) with external inputs and coupling factors (S). If all external and coupled inputs are set to be zero, then all S-portals are zero. In this case, Eq. 2-15 is reduced to

$$\dot{r} = wr(1 + S_\alpha - r^2). \quad \text{Eq. 2-17}$$

From the first order ODE of the amplitude, r has two equilibriums ($r = 0$ and $r = 1$). Here, $r = 0$ is an unstable point, $r = 1$ is a stable point. Next, consider the phase equation is given the same assumption, the new equation from Eq. 2-16 is

$$\dot{\varphi} = w. \quad \text{Eq. 2-18}$$

This means that the phase is advancing at a constant rate and also the intrinsic frequency. If the possibility of the stimuli that affects the phase is considered, the equation needs to incorporate refractoriness (R) (Zalay & Bardakjian, 2008). This can be implemented as a

Butterworth highpass filter (Eq. 2-19) such that the pulse advance will not be affected when the phase is small. In the function equation, r_1 , r_2 , and r_3 are parameters controlling the magnitude, phase-cutoff and order of the filter.

$$R(\varphi) = \frac{1}{\sqrt{1 + \left(\frac{2\pi r_1}{\varphi}\right)^{r_2}}}. \quad \text{Eq. 2-19}$$

Finally, the state space information is mapped onto the membrane voltage using static nonlinearity (Zalay & Bardakjian, 2008),

$$y = a_0 + A(S_p) + rW(\varphi). \quad \text{Eq. 2-20}$$

The bias voltage (a_0) sets the mean voltage level of the oscillator unit (which represents the resting potential of a given neuron). The mapping function (W) (Figure 2-11) is the intrinsic voltage waveform of the oscillator, which depends uniquely on the phase. The basic procedure for identifying the waveform involves performing a patch clamp or extracellular field recording, isolating a characteristic waveform from the signal (with zero mean), normalizing it to the values in the phase over the interval 0 to 2π in such a way that the beginning of the waveform corresponds to $\phi = 0$, and creating a lookup table so that the values of W are tabulated against the value of ϕ . Since r is supposed to be around 1 most of the time, a multiplier is given to account for slight variations in the action potential amplitude.

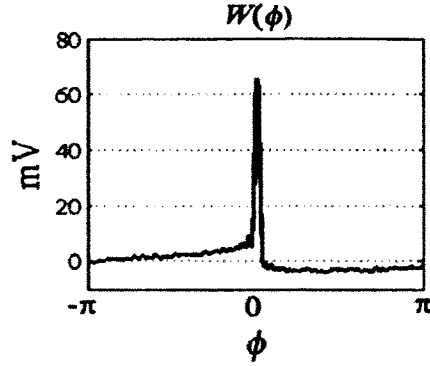


Figure 2-11: The intrinsic waveform the MCO model (Zalay & Bardakjian, 2008).

Four types of stimuli shown in the model flow map (Figure 2-12) that can affect the oscillator are:

- Synapse (S_ρ) (Zalay & Bardakjian, 2008):

$$S_\rho = \sum_{m=1}^M \left(\frac{c_\rho (y_m - a_{0,m}) V (y_m - a_{0,m})}{\sigma_n} \right) + S_{\rho,ext}. \quad \text{Eq. 2-21}$$

If the presynaptic cell does not have an AP, there is no postsynaptic response. V can be treated as a highpass filter in which it sets the threshold to determine if the pre-synaptic cell has an AP. The coupling factor c accounts for the location of the synapse (spatial information) or efficacy of the synapse. Also, the post-synaptic effect is accounted for through a convolution function as follows (Zalay & Bardakjian, 2008),

$$A(S_\rho(t)) = \frac{RMS(W(\varphi))}{100} \int_{t_0}^t a S_\rho(u) \cdot (t - u) \exp\{1 - a(t - u)\} du. \quad \text{Eq. 2-21}$$

- Electric field (ϕ) and extra-synaptic chemical coupling (α): Both portals utilize the same form of the equation (Zalay & Bardakjian, 2008):

$$S_\rho = \sum_{m=1}^M \left(\frac{c_\rho (y_m - a_{0,m})}{\sigma_n} \right) + S_{\rho,ext}. \quad \text{Eq. 2-22}$$

- Gap junction (γ):

The gap junction is complex. The internal clock variables of coupled MCOs are accessed directly by the gamma-portal, bypassing the mapper. The n^{th} MCO is a network of n oscillators.

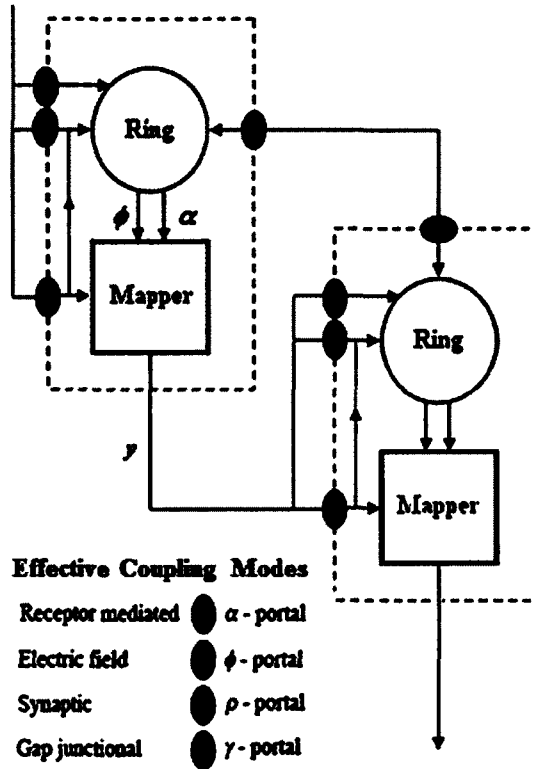


Figure 2-12: The flow map of the MCO model (Zalay & Bardakjian, 2008).

This method for generating an output waveform is very versatile because it can accommodate any biological waveform shape, and the waveform can be recorded from any source, though mathematically the function is not analytic. Another interesting note on using the oscillator to model the neurons is that some neurons exhibit autonomous oscillatory behavior (e.g., some CA3 pyramidal cells). Even though conductance based models and some integrate-and-fire models can generate pulse trains, they usually require a constant DC current injection.

The second type of oscillator is called the Labile clock (Figure 2-13) in which the neuron still behaves like an oscillator, but it will only be active as long as the input (X) is above a designated threshold. It maintains its active level as long as the stimulus is presented. This type of clock is defined by the amplitude and phase equations and the mapping function translates r and ϕ into the voltage (y). The only difference between the Labile clock and the oscillator model is in the amplitude equation (Zalay & Bardakjian, 2008):

$$\dot{r} = k_{\alpha} r^{1/3} (v(X) - r^2) + S_{\gamma 1} \sin(\varphi) + S_{\gamma 2} \cos(\varphi). \quad \text{Eq. 2-23}$$

The input X contains two coupling factors (α and ρ) (Zalay & Bardakjian, 2008):

$$X = K_{\alpha} S_{\alpha} + K_{\rho} A(S_{\rho}). \quad \text{Eq. 2-24}$$

The phase and mapping equations are the same as before since the phase of the Labile clock keeps advancing in the same manner as the oscillator.

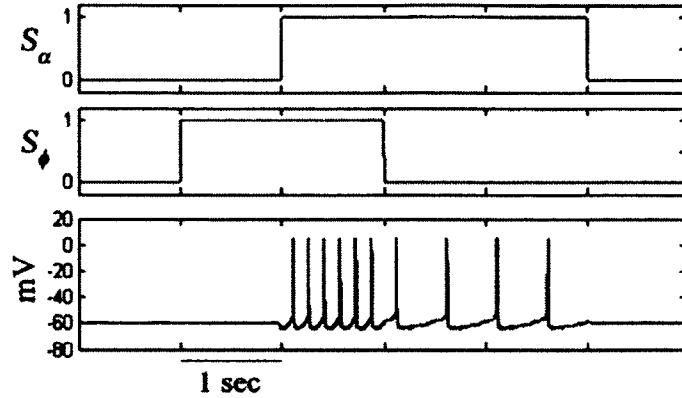


Figure 2-13: The model output of the Labile clock (Zalay & Bardakjian, 2008).

The third type of unit of MCO model is the hourglass (Figure 2-14) which can be considered as an intermediate neural output. The equations are (Zalay & Bardakjian, 2008):

$$\dot{r} = -k_{\alpha}r^{1/3}(1 - g(\varphi) - r^{1/3})(U - g(\varphi) - r) + X(1 - r), \quad \text{Eq. 2-25}$$

$$\dot{\varphi} = k_{\varphi 1}r - k_{\varphi 2}\varphi(1 - r)^{100} + X(1 - r). \quad \text{Eq. 2-26}$$

For the Gaussian function ($g(\phi)$) near 0, the limit cycle is at $r = 0$ and there is a repeller at the threshold (U). The effective driving stimulus (X) is multiplied by $(1-r)$ so that the hourglass model exhibits refractoriness when it is active. It remains insensitive until $r \ll 1$. If $r < U$, then the amplitude tends toward 0. The phase will advance as long as r is large, but $g(\phi)$ will pull r back inside the circle radius U . The resetting of the phase is achieved with the ϕ in the middle term. When r goes to 0, the phase will remain near the peak location (ϕ_{hys}) of the Gaussian function so that the next activation cycle would not begin again at $\phi = 0$, but would start from where the phase last stopped. To bring the phase back to 0 only when $r \ll 1$ requires phase resetting. If r is near 1 (active), no phase resetting occurs. The g -function determines the duration of the ON-cycle in the hourglass

dynamic by modifying the amplitudes of the attractor limit cycles (Zalay & Bardakjian, 2008):

$$g(\varphi) = \frac{G}{\Delta\varphi} \exp\left(-\frac{\varphi - \varphi_{hys}^2}{2(\Delta\varphi)^2}\right). \quad \text{Eq. 2-27}$$

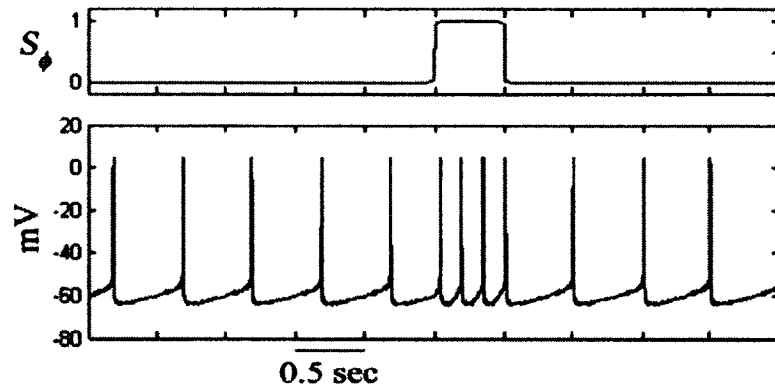


Figure 2-14: The model output of the hourglass (Zalay & Bardakjian, 2008).

2.4 Seizure Stimulation Methods

Epilepsy is studied on different levels ranging from ion channel kinetics to EEG signals. For the EEG level, researchers use the responsive stimulation feedback control system (Figure 2-15). The mechanism of this kind of feedback is to maintain the normal frequency level for the neurons. Therefore, this feedback control system can sense seizure activity and suppress it (Chakravarthy et al., 2009; Colpan et al., 2007). Other researchers have used chemical or electrical means to induce seizure events or seizure-like activities in animal brain slices or a cultured neuron (Wagenaar et al., 2005; Isomura et al., 2008). For example, van Drongelen et al. (2007) used an electrical stimulator to disperse seizure spiking in neurons cultured on a microelectrode array (MEA). This technique allowed them to track the seizure propagation through the cells on the MEA. Other stimulation methods have been developed to reduce seizure activity such as closed-loop stimulation

(Wagenaar et al., 2005), controlled pulse stimulation (Albensi et al., 2008), and high-frequency stimulation (Su et al., 2008). These stimulation protocols are then typically incorporated as a component in systems that monitor EEG activity and attempt to control seizures.

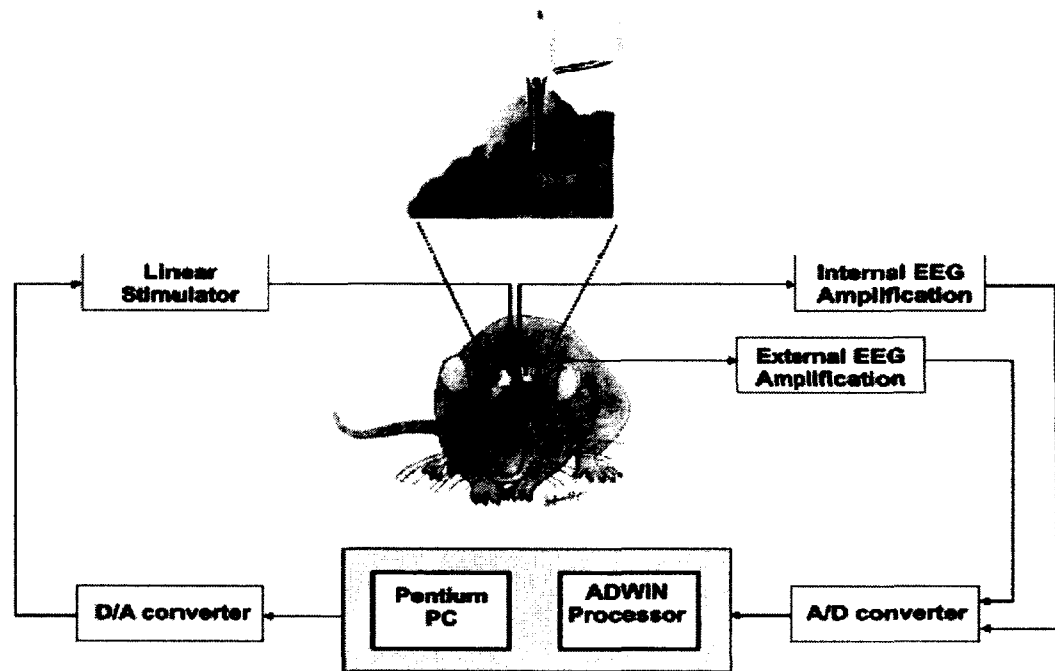


Figure 2-15: EEG seizure control feedback system using the responsive stimulation (Colpan et al., 2007).

Since neuronal communication in the hippocampus is quite complex and seizure involving the hippocampus is difficult to understand, researchers model this interaction as a small neural network or specific neuron pattern for research purposes (Wagenaar et al., 2005). Various nonlinear models of the hippocampus (Courellis et al., 2006) and neuron bursting patterns (Hemond et al., 2008) have also been used in models of hippocampal networks. Different neuron firing patterns (Izhikevich, 2004) have been used to model

seizures, but seizures seem to be unexpected ruleless phenomena and no single firing pattern has been found to describe them.

Just as researchers reduced the size of their computational models to simplify a complex system, EEG seizure researchers often use brain slices or cultured networks of the neurons to simplify their biological models. In this case, seizure can be controlled and induced by different chemicals such as low-Mg, 4-Aminopyridine (4-AP, block of the potassium current), kainic acid and/or a high-potassium solution (Kasugai et al., 2007; Khosravani et al., 2005; Luhmann et al., 2000; Traynelis & Dingledine, 1988). In a typical rat brain slice model, the CA3 region of the hippocampus exhibited spontaneous electrographic seizure and then propagated to the CA1 region throughout the pyramidal cells (Traynelis & Dingledine, 1988). Such experimental data can facilitate seizure modeling and development of a feedback control system for the understanding and treatment of seizures.

CHAPTER 3

METHODS

This chapter describes all the methods used in this dissertation including *in vitro* data acquisition, *in vitro* slice seizure model, the computational seizure model, seizure stimulation tools, and statistical analysis. They were applied to accomplish the tasks of seizure activities modeling and seizure-like event (SLE) stimulation. Statistical analysis helps to verify the results.

3.1 *In Vitro* Data Acquisition

In the low-Mg²⁺ model of epilepsy, Mg²⁺ blockade of post-synaptic N-methyl-D-aspartate (NMDA) receptor channels and magnesium-sensitive Ca²⁺ channels is reduced, thus increasing the network susceptibility to depolarizing influences, as well as decreasing membrane charge-screening effects (Derchansky et al., 2004). Hence, network hyper-excitable conditions can be produced.

The experimental procedures used in this study were approved by the Tulane University Institutional Animal Care and Use Committee. Four male Wistar rats, three to four weeks old, were decapitated under deep isoflurane anesthesia and their brains were rapidly extracted and placed in ice-cold (~1 °C), oxygenated (95% O₂, 5% CO₂) artificial cerebrospinal fluid (aCSF) solution containing (in mM): 123 NaCl, 3.3 KCl, 1.5 CaCl₂, 2 MgSO₄, 24 NaHCO₃, 1.2 NaH₂PO₄, and 25 glucose (pH 7.4) for five minutes. Transverse

hippocampal slices (Figure 3-1) (300 μm) were sectioned and transferred immediately into a storage chamber, where they were perfused with oxygenated aCSF solution and maintained at room temperature for one hour.

Afterwards, a single slice at a time was moved to a recording chamber on an upright microscope (Olympus) and perfused with aCSF, bubbled with 95% O_2 and 5% CO_2 , using a peristaltic pump (Ismatec, Glattbrugg, Switzerland) at a rate of two ml/min. Whole-cell patch-clamp recordings of pyramidal neurons in the CA1 region were conducted in the current-clamp mode under visual control using infrared light and differential interference contrast optics. Glass micropipettes having a tip resistance 4-5 $\text{M}\Omega$ were pulled on a horizontal puller (Sutter Instr) and filled with (in mM) 135 K-Gluconate, 10 NaCl, 1 MgCl_2 , 2 Na_2ATP , 0.3 NaGTP (Tris), 10 NaHEPES, 0.5 EGTA and 0.0001 CaCl_2 (PH 7.4). Recordings were performed with a MultiClamp 700 amplifier and PClamp 10 software (Molecular Devices, Sunnyvale, CA). An initial 10-min stabilization period was provided before starting the recordings. Normal neuron activity was recorded using a standard aCSF solution for the first 10 minutes of recordings. The standard aCSF was then replaced with a modified aCSF solution containing a low magnesium concentration (0.25 mM instead of 2 mM MgSO_4), which was applied for at least one hour. The standard aCSF solution was then reapplied for another 15 minutes as the washout condition. All the datasets were sampled at 500 Hz after they were subjected to a built-in anti-aliasing lowpass filter (corner frequency 200 Hz) using Clampfit 10.2 software (Molecular Devices, Sunnyvale, Ca).

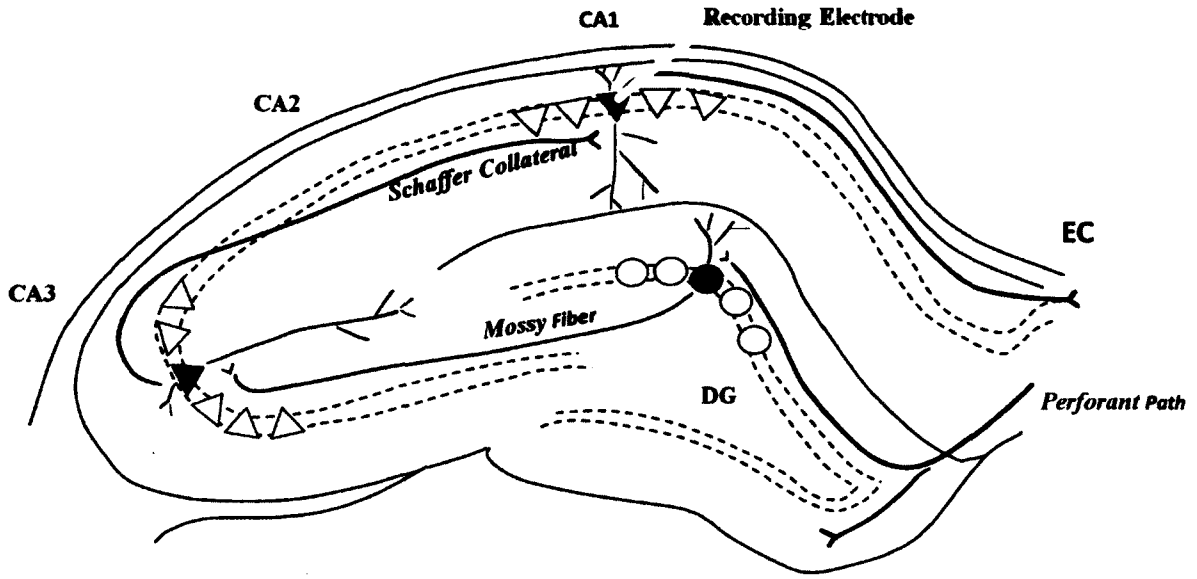


Figure 3-1: A schematic illustration of a transverse hippocampal slice (Freund & Buzsaki, 1996). Whole-cell patch-clamp recordings of pyramidal neurons were conducted in the cell body layer of the CA1 hippocampal subfield.

3.2 Model Description

The modeling of *in vitro* hippocampal slices exhibiting SLEs was achieved using the Cognitive Rhythm Generator (CRG) SLE model (Zalay & Bardakjian, 2009; Zalay et al., 2010). The amplitude and phase information of the limit cycles can be adjusted, enabling various complex state space geometries. The CRG model uses mode outputs that are combined via static nonlinear functions to incorporate nonlinear input coding functionality to modulate the excitability of the network. Excitatory pyramidal neuron and inhibitory interneuron subpopulations of the hippocampal CA1 region can be represented using networks of four reciprocally connected model units. The dynamics of each unit can be defined by four differential equations defining the state space of the system. These state variables can then be mapped nonlinearly to generate the transmembrane potentials based on the action potential waveform that has been recorded and stored previously.

The CRG model was modified to enable each unit to behave either as an oscillator that can generate an action potential (AP) train without any external stimulation or as a threshold-based unit that only triggers an AP when the input is sufficiently large. Each CRG unit contains three components: a clock, a mapper, and a mode bank. The clock, described by Eq. 3-1 and Eq. 3-2, can undergo phase advancement depending on the intrinsic angular frequency (w_n). The state variables u_{1n} and u_{2n} describe the limit cycle stage of the oscillation dynamics. Eq. 3-3 and Eq. 3-4 give the differential equation representation of the synaptic function. It has an equivalent functionality of a first-order kernel, implemented as an exponential impulse response function, connecting the outputs of other model units. The modified equations of the n^{th} oscillatory unit are:

$$u_{1n} = w_n \{ u_{2n} (1 + S_{\varphi,n}) + u_{1n} (V(x) - u_{1n}^2 - u_{2n}^2) \}, \quad \text{Eq. 3-1}$$

$$u_{2n} = w_n \{ -u_{1n} (1 + S_{\varphi,n}) + u_{2n} (V(x) - u_{1n}^2 - u_{2n}^2) \}, \quad \text{Eq. 3-2}$$

$$u_{3n} = u_{4n}, \quad \text{Eq. 3-3}$$

$$u_{4n} = \beta_n F_n - 2\beta_n u_{4n} - \beta_n^2 u_{3n}, \quad \text{Eq. 3-4}$$

where β_n is the kernel duration and $S_{\varphi,n}$ is the phase modulation function. The limit cycle of each CRG unit is defined by the function $V(x)$. Previous implementation of an oscillator unit from the CRG SLE model consisted of a constant $V(x) = 1$. Our modified CRG model allows the limit cycle magnitude to change depending on the external driving force to the unit. Units One and Two are kept as oscillators with $V(x) = 1$. The inhibitory Units Three and Four are threshold-based units with $V(x)$ controlled by the driving stimulus x , which is related to the receptor level X and the synaptic function u_{3n} .

$$V(x) = v_1 / (1 + e^{-v_2(x-v_3)}), \quad \text{Eq. 3-5}$$

$$x = 8u_{3n} + X, \quad \text{Eq. 3-6}$$

where v_1 , v_2 and v_3 are the magnitude, slope and threshold. The coupling between CRG units can be achieved in two ways: electric field related coupling as described by Eq. 3-7 and synaptic coupling as described in Eq. 3-8 (Zalay et al, 2010):

$$S_{\varphi,n} = c_{0n} + k_n u_{3n} + f_n(t), \quad \text{Eq. 3-7}$$

$$F_n = \sum_{m=1}^M c_{mn} y_m + i_n(t). \quad \text{Eq. 3-8}$$

The field coupling portal depends on the modulation gain k_m , the coupling offset c_{0n} and an optional additive electric field input $f_n(t)$. The parameter c_{mn} gives the coupling coefficient from unit m to unit n . The function $i_n(t)$ is the external electrochemical input which is set to be zero in this simulation. Finally, the nonlinear mapper function gives the output:

$$Y_n = c_{0n} + u_{3n} + \left(\sqrt{u_{1n}^2 + u_{2n}^2} \right)^{20} W \left(\tan^{-1} \frac{u_{2n}}{u_{1n}} \right), \quad \text{Eq. 3-9}$$

where the function W is the intrinsic action potential waveform. The power 20 in the amplitude is created so that state variables (u_{1n} , u_{2n}) not sufficient to trigger action potentials will have little impact on the electrochemical interaction described in Eq. 3-8. The CRG model used in this study consisted of four units (Figure 3-2). The first two units formed auto-associative excitatory connections with each other as well as uni-directional excitatory connections to Units Three and Four. They also received inhibitory feedbacks from Units Three and Four.

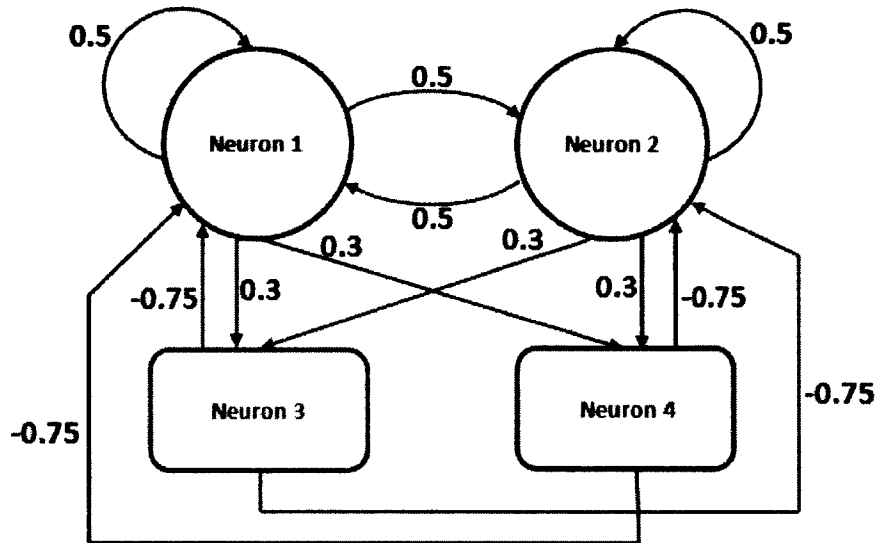


Figure 3-2: A four-unit CRG model consisting of two excitatory units (one and two) and two inhibitory units (three and four) along with the coupling coefficients are illustrated. Units Three and Four are also threshold-based units.

A detailed list of the parameters along with their values used in the simulations is shown in Table 3-1. Different excitability parameters (β ranging from 1 to 20, k from 1 to 30, and X from 0 to 5) were used to evaluate how the system LPR dynamics related to SLEs can be affected. Furthermore, the ratio of k/β , proportional to the area under the first-order kernel characteristics was also studied. For each (β, k, X) combination, up 3-minutes of simulation were performed. The relationship between the model parameters (β, k, X) and the characteristics of the model dynamics (firing rate, the mean duration, and the overall percentage of time that the model dynamics remained in the LPR mode) were quantified using Pearson correlation coefficient analysis. The firing rate was defined as the inverse of the average peak-to-peak distance of the action potential train in the LPR SLE mode, defined as the period of time in which the slice or the model exhibited significantly lower maximum Lyapunov exponent in the interspike interval diagram (Wolf et al., 1985). This definition is consistent with experimental evidence of a drop in

dynamic complexity associated with seizure epochs (Chiu et al., 2006b). The maximum Lyapunov exponent for the interictal region was found to be 1.75 ± 0.11 (biological field data) and 1.43 ± 0.15 (modified model), while in the ictal region, the maximum Lyapunov exponent was computed to be 0.192 ± 0.141 (biological field) and 0.280 ± 0.207 (modified model). In both cases, the complexity of the interictal and ictal activities are significantly different statistically (T-test, $p < 0.01$ in both biological and model data).

Table 3-1: Model parameter symbols, explanations, and values used in the simulations

Type	Symbol	Description	Values																
Network Size	M, N	Number of the cell unit	4																
Unit Characteristics	w_n	Intrinsic oscillator frequency	[4.23 4.14 4.65 4.56]																
	c_{0n}	Constant offset	[-0.2 -0.2 0 0]																
	$W(\varphi)$	Intrinsic output waveform	-																
Network Connection	c_{mn}	Coupling coefficient from unit m to n	<table border="1" style="display: inline-table; vertical-align: middle;"> <tr> <td>0.5</td> <td>0.5</td> <td>-0.75</td> <td>-0.75</td> </tr> <tr> <td>0.5</td> <td>0.5</td> <td>-0.75</td> <td>-0.75</td> </tr> <tr> <td>0.3</td> <td>0.3</td> <td>0</td> <td>0</td> </tr> <tr> <td>0.3</td> <td>0.3</td> <td>0</td> <td>0</td> </tr> </table>	0.5	0.5	-0.75	-0.75	0.5	0.5	-0.75	-0.75	0.3	0.3	0	0	0.3	0.3	0	0
0.5	0.5	-0.75	-0.75																
0.5	0.5	-0.75	-0.75																
0.3	0.3	0	0																
0.3	0.3	0	0																
Threshold Function	v_1	Magnitude	1																
	v_2	Slope	30																
	v_3	Threshold	0.5																
Excitability	β_n	Mode decay constant	Vary 1 to 20																
	k_n	Modulatory gain	Vary 1 to 30																
	X	DC component (receptor level)	Vary 0 to 5																
Optional Inputs	$f_n(t)$	Field related input	0																
	$i_n(t)$	Electrochemical input	0																
Unit Output	y_n	Output of model unit	-																

3.3 Statistical Comparison

The *in vitro* experimental data was later partitioned into 3-minute non-overlapping time windows after the identification of the ictal onsets. The CRG model outputs at different (β , k , and X) combinations were generated. The inter-spike interval (ISI) distributions of the *in vitro* experimental data and the CRG model outputs were created and compared using histogram analysis. If the ISI pair contained an overlapped area of over 80%, they were then sent to the critical statistical test. The testing process consisted of the application of a bootstrap technique to the Fasano-Franceschini statistic (Fasano & Franceschini, 1987).

Two bivariate groups, denoting the biological and model data respectively, have been compared. The successive ISI of each group, mapped on a two-dimensional space (ISI index t , ISI index $t+1$) = (x, y) , can be expressed as $\{(x_i^{(1)}, y_i^{(1)}), i = 1, \dots, m\}$ and $\{(x_i^{(2)}, y_i^{(2)}), i = 1, \dots, n\}$. The values m and n denote the number of ISI samples in group 1 and 2, respectively. We tested whether the two ISI groups came from one common population/distribution. The Null Hypothesis was that the two ISI groups come from one distribution. The simplified Fasano-Franceschini statistic was defined as:

$$FF = \max \{T_1, T_2, T_3, T_4\}. \quad \text{Eq. 3-10}$$

The two-sample Kolmogorov-Smirnov statistic (T_q) for each quadrate ($q = 1$ to 4) of the 2-D ISI distribution was defined as the maximum difference between the empirical bivariate distribution function of each group:

$$T_q = \max_{j=1}^{m+n} \{D_1^{(q)}(x_j, y_j) - D_2^{(q)}(x_j, y_j)\}. \quad \text{Eq. 3-11}$$

The common distribution $\{(x_j, y_j), j = 1, \dots, m + n\}$ was defined as:

$$\{(x_{1i}, y_{1i}), i = 1, \dots, m\} \cup \{(x_{2i}, y_{2i}), i = 1, \dots, n\}. \quad \text{Eq. 3-12}$$

The empirical bivariate distribution functions for the first group were then given as:

$$D_1^{(1)}(x_j, y_j) = \#\{x_{1i} \leq x_j, y_{1i} \leq y_j\} / m, \quad \text{Eq. 3-13}$$

$$D_1^{(2)}(x_j, y_j) = \#\{x_{1i} \geq x_j, y_{1i} \leq y_j\} / m, \quad \text{Eq. 3-14}$$

$$D_1^{(3)}(x_j, y_j) = \#\{x_{1i} \leq x_j, y_{1i} \geq y_j\} / m, \quad \text{Eq. 3-15}$$

$$D_1^{(4)}(x_j, y_j) = \#\{x_{1i} \geq x_j, y_{1i} \geq y_j\} / m. \quad \text{Eq. 3-16}$$

The empirical bivariate distribution functions for the second group followed the above formulations (Eq. 3-13 to Eq. 3-16):

$$D_2^{(1)}(x_j, y_j) = \#\{x_{2i} \leq x_j, y_{2i} \leq y_j\} / n, \quad \text{Eq. 3-17}$$

$$D_2^{(2)}(x_j, y_j) = \#\{x_{2i} \geq x_j, y_{2i} \leq y_j\} / n, \quad \text{Eq. 3-18}$$

$$D_2^{(3)}(x_j, y_j) = \#\{x_{2i} \leq x_j, y_{2i} \geq y_j\} / n, \quad \text{Eq. 3-19}$$

$$D_2^{(4)}(x_j, y_j) = \#\{x_{2i} \geq x_j, y_{2i} \geq y_j\} / n. \quad \text{Eq. 3-20}$$

The Fasano-Franceschini test statistic (FF) was computed using Eq. 3-10 given the original two groups. The data from the two groups were then combined to form a single group with the size $m + n$. Two bootstrap (or random groups) with replacement from the combined data were performed and the new bootstraps simplified Fasano-Franceschini test statistic (FF_b) was computed. The process was repeated 500 times (for b ranging from 1 to 500). The P-value defined the significance level in which the Null Hypothesis could be rejected was computed as:

$$P = \#\{FF_b \geq FF\} / 500. \quad \text{Eq. 3-21}$$

If the P-value fell below 0.05 (the level of significance), then we rejected the Null Hypothesis in favor of the Alternative Hypothesis that the two groups belonged to two different parent populations. Otherwise, we accept the Null Hypothesis.

3.4 *In Vitro* Hippocampal Slice Seizure Model

The experimental procedures used in this study were approved by the Louisiana Tech University Institutional Animal Care and Use Committee. Male Sprague Dawley rats were anesthetized with CO₂ and sacrificed at four to six weeks of age. Their brains were rapidly dissected and placed into ice-cold (~1 °C), oxygenated (95% O₂, 5% CO₂) artificial cerebrospinal fluid (aCSF) solution for 5 minutes. The aCSF solution contains (in mM): 123 NaCl, 2.5 KCl, 1.5 CaCl₂, 2 MgSO₄, 24 NaHCO₃, 1.2 NaH₂PO₄, and 25 glucose (pH 7.4). The hippocampus was dissected, and 300 µm transverse slices were sectioned and transferred immediately into a storing chamber with ice-cold, oxygenated aCSF solution and maintained at room temperature for one hour. The Mg-free aCSF solution, consisted of the same aCSF recipe without the MgSO₄, was applied after the slice has been stabilized and transferred to the multi-electrode array (MEA) (Multi Channel Systems, Reutlingen, Germany). The electric field potential was obtained near the pyramidal neurons in CA1 region of the hippocampal slices (see Fig. 1). The data was then lowpass anti-aliasing filtered at 400 Hz and sampled at 1 kHz for further analysis.

3.5 Modified Cognitive Rhythm Generator Model

For the simulation of the electric field potential of the Mg-free *in vitro* hippocampal slice, a modified cognitive rhythm generator (CRG) model was used. The CRG model utilized the experimentally determined input-output kernel functions to modulate the unit and network excitability. The main parameters in the kernel function,

representing the mode decay constant, modulatory gain, and receptor level have been carefully studied (Iasemidis et al., 2004) to reproduce the different dynamics that exists in the manifestation of seizure episodes in the in vitro hippocampal slice preparation. Subpopulations of the hippocampal CA1 region can be represented using networks of four reciprocally connected model units. The state variables of each unit can then be mapped nonlinearly to generate the transmembrane potentials based on the action potential waveforms previously recorded. In order to estimate the field recording signal from the model, each neural unit signal was twice differentiated and then added together, as shown in Figure 3-3.

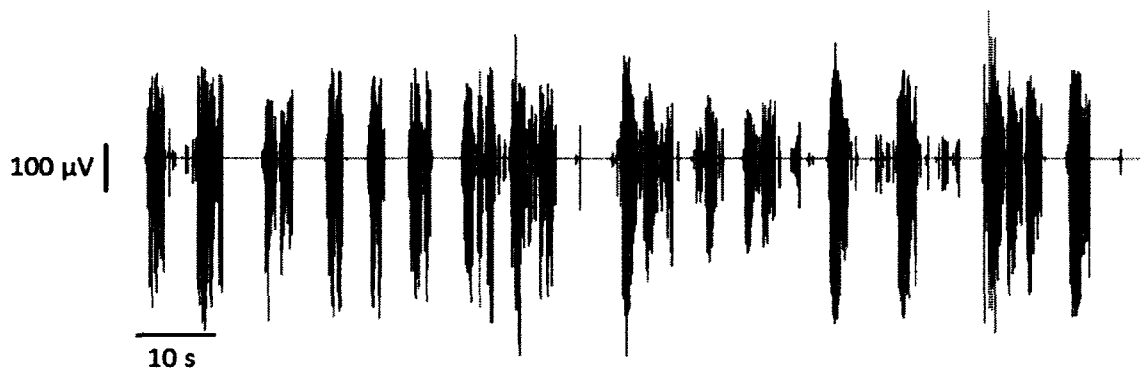


Figure 3-3: Simulated field potential generated using the modified CRG model, illustrating spontaneous generation and termination of SLEs.

3.6 Field Stimulation

Spontaneously generated SLEs can be terminated by the process of neural resetting. It is therefore, in our hypothesis, to evaluate whether the intrinsic characteristics of the neural activities may hold a possible key to SLE suppression strategy. Furthermore, recent study on a computer simulated seizure model indicated that model based electrical stimulation is helpful to seizure control (Colic et al., 2011). Here, it is also natural to speculate that the mechanism in which the neural resetting takes place

may be found at the termination of a seizure episode, called the post-ictal activity. In previous research, our group has shown that the state transitions associated with SLEs spontaneously triggered by Mg-free experimental condition can be represented by the modified CRG model with different parameter combinations (Iasemidis et al., 2004). Three different CRG-generated postictal activities were selected (Figure 3-4) and scaled to a range of $\pm 200 \mu\text{V}$, similar to the physiological recorded data amplitude. These oscillator-model generated signals were treated as field potential stimulation to the slice preparation through the MEA, when the onsets of SLEs were detected (accompanied by an increase in spiking frequency and a reduction in signal complexity). One of the three candidate postictal signals was randomly selected. Next, the periodic bipolar square-wave pulses with a 10 Hz frequency and a 9% duty cycle were used as the stimulus to carry out the contrast experiment. Finally, a two-sided rank sum test was performed on the inter-seizure interval to evaluate the Null Hypothesis that the negative control (NC), postictal stimulation (PS), and bipolar pluses (BP) stimulation come from the distributions with equal medians.

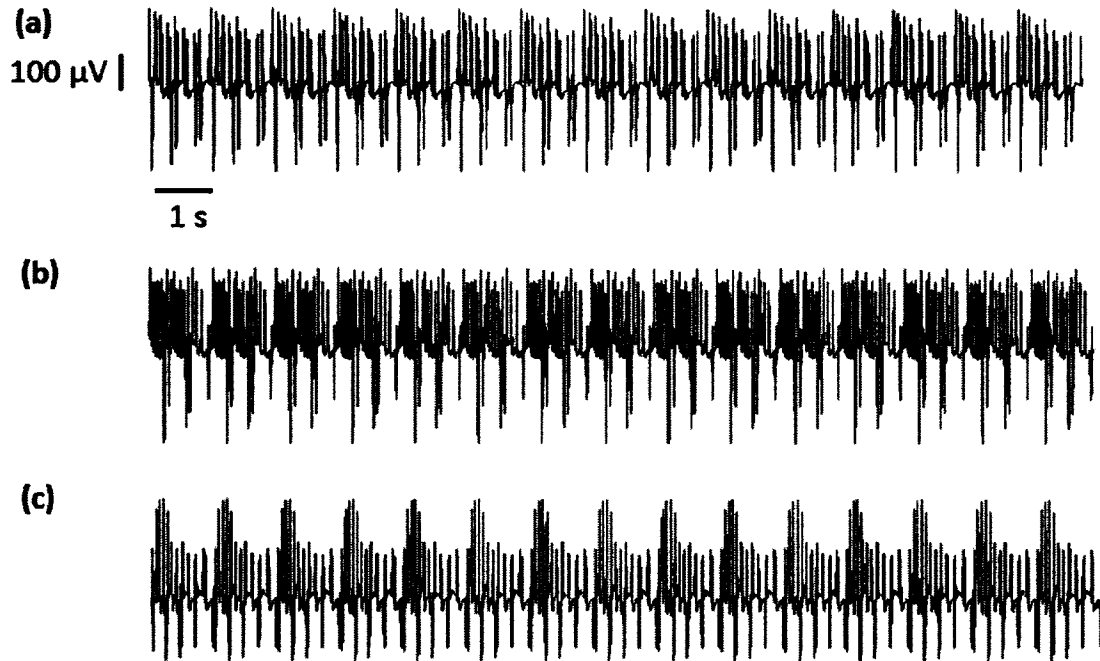


Figure 3-4: Oscillator-based postictal field data was repeated to create the stimulation signals that are 15-seconds in length.

CHAPTER 4

RESULTS

This chapter presents the various patterns of seizure-like activities that are obtained when the cognitive rhythm generator is modified under different conditions. The seizure model output is matched to the data collected from the *in vitro* slice seizure model. P-value test helps to quantify the fitting results statistically. Results from Sections 4.1-4.3 have been published in *Journal of Network: Computation in Neural Systems*. Results from Sections 4.4-4.5 have been accepted by *IEEE EMBS Annual International Conference Proceedings 2012*.

4.1 Threshold-Based Oscillation Model Output

A network of two oscillators coupled with two threshold-based units was able to generate state transitions into and out of ictal events similar to those observed in *in vitro* low-Mg²⁺ hippocampal slices. An improvement in enhancing the similarity between the model output and the biological data can be achieved after the proposed modifications. The original CRG SLE model was configured such that spontaneous seizure activity can be generated. Silent periods without spiking can indeed be generated in the original model with the appropriate choice of coupling values and with the addition of refractoriness. In this work, one of the main foci was on reproducing single neuron AP dynamics. Once the threshold-based oscillatory function was implemented with the $V(x)$

function, the radii of the limit cycles were allowed to vary between 0 and 1, depending on the excitation level. This way, threshold-based oscillation can be achieved without creating a different set of equations from endogenous oscillators.

Different combinations of the parameters directly related to network excitability (β , k , and X) were used to evaluate how the dynamics of the model network can be affected. Characteristics that described the higher frequency LPR spiking region, similar to the SLEs, such as the mean firing rate and the mean duration were quantified and summarized in Figure 4-1. Smaller β , larger k , and larger X all led to higher mean firing rate, corresponding to the modeling of frequency features of the SLEs. The excitation ratio (k/β) was found to be most positively correlated ($r = 0.9810$; $p < 0.001$) with the mean firing rate in the LPR mode (slope = 0.316). In general, β parameter is more strongly correlated to the overall percentage of time that a network stays in the LPR mode ($p < 0.05$). The k parameter is correlated to the average duration of the LPR mode ($p < 0.05$). The firing pattern dynamics as a function of β , k , and X is shown in Figure 4-2.

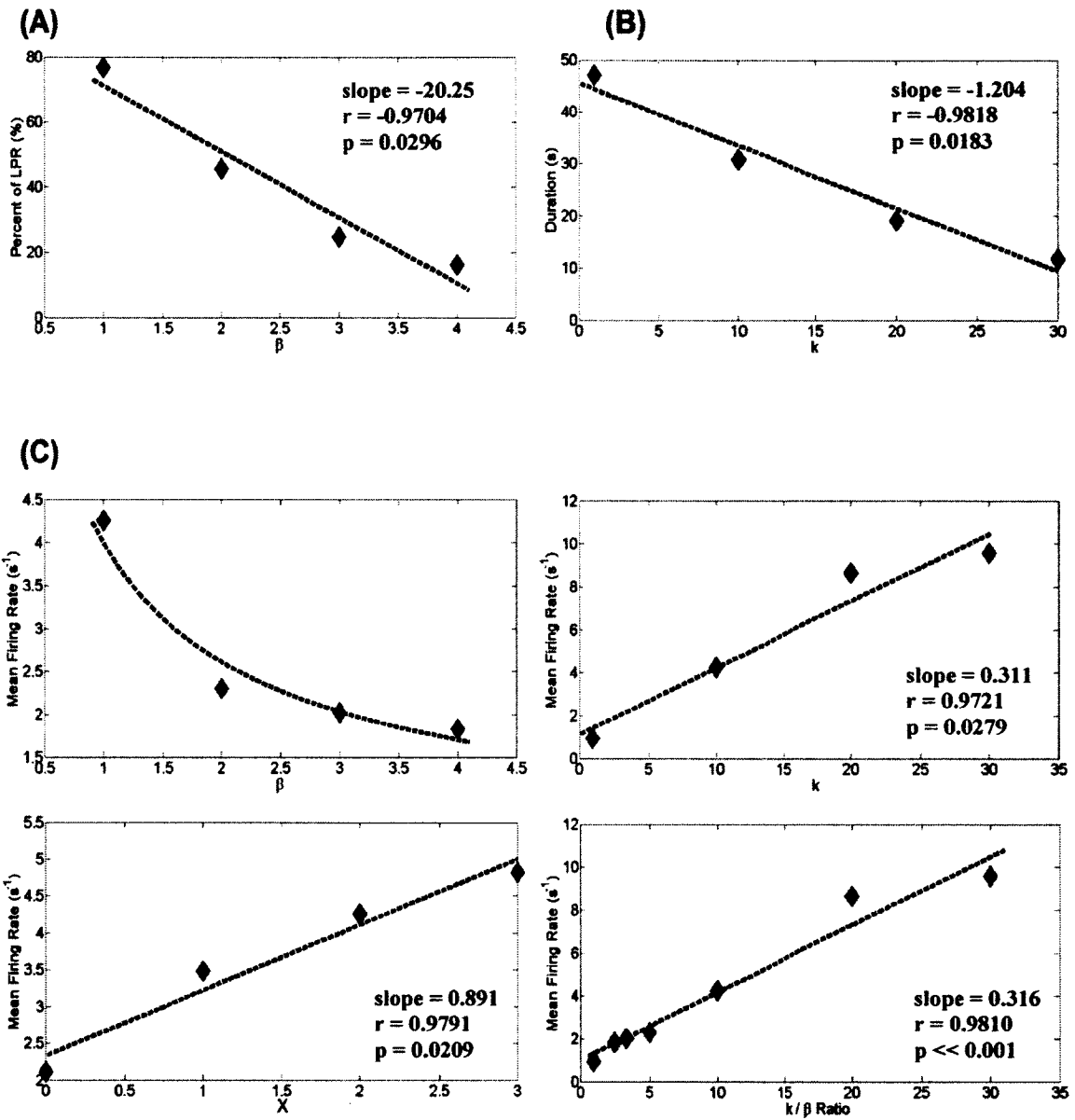


Figure 4-1: The mean firing rate and the mean duration of the LPR mode, were evaluated as a function of β , k , X , as well as the excitation ratio of k/β . All of the analyses were performed on the model output signal from Unit One. (A) The overall percentage of time that a system stays in the LPR mode is most correlated to the kernel duration ($p < 0.05$). (B) The modulation gain affects the average duration of the LPR mode negatively ($p < 0.05$). (C) The modulation gain, excitation ratio, and DC excitation level are positively correlated to the mean firing rate within the LPR mode (Pearson correlation coefficient: $r = 0.9721$, 0.9810 and 0.9791 , respectively; $p < 0.05$, $p < 0.05$ and $p << 0.001$, respectively). The mean firing rate is also found to be inversely proportional to the kernel duration.

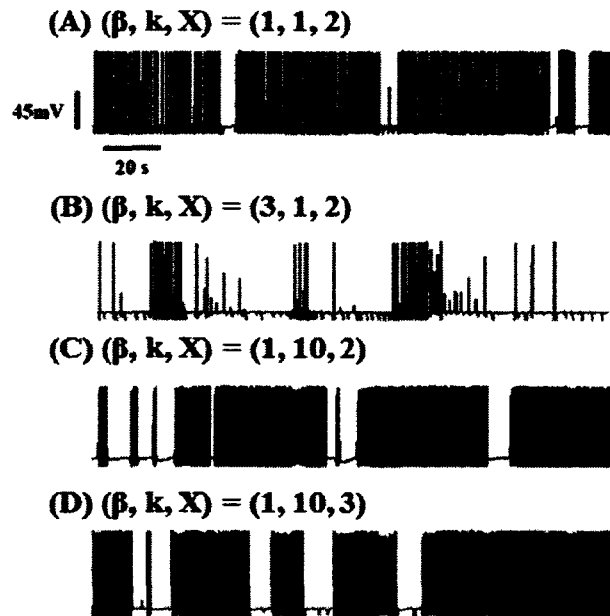


Figure 4-2: The model outputs (from Unit One) are illustrated for different combinations of β , k , and X . Using (A) as the control, the parameters were changed one at a time. The parameters β and k both control the firing rates. (B) The mean firing rate decreases with an increasing β , while a larger k leads to a higher firing rate (C). (D) The parameter X mainly affects the firing pattern switching, and can also slightly increase the mean firing rate.

4.2 Low-Magnesium Seizure-Like Activity Simulation

In the previous analysis of the CRG SLE model (Zalay et al., 2010), only the interictal and ictal dynamics were considered in the state space analysis. The dynamics of possible preictal activity and how the excitability of the CRG model may be used to describe these state transitions were evaluated here. The modified CRG model was able to simulate three different states: preictal, ictal and postictal state by changing the values of parameters β , k , and X (Figure 4-3). Table 4-1 summarizes the best fit biological and model data having the largest P-values obtained using the Fasano-Franceschini statistic. The neuron excitability dynamics of the computational simulation was also estimated to be proportion to the ratio of k/β . The excitability increased when the SLE transitioned from preictal to ictal state and decreased in the postictal state.

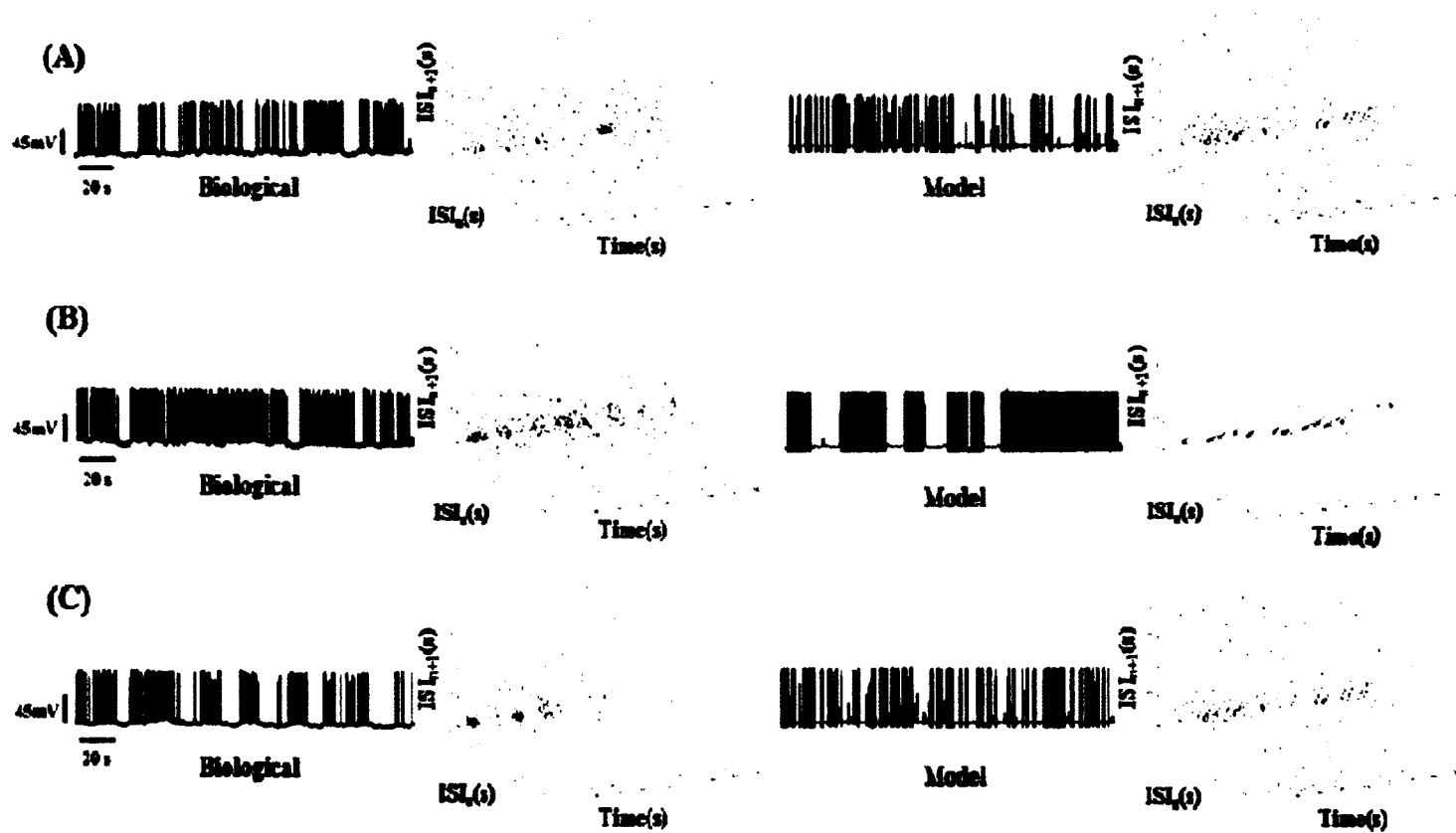


Figure 4-3: Matching the biological data with the CRG model output during (A) preictal, (B) ictal, and (C) postictal activities. The time varying ISI plot for each condition is also shown. The major differences between the different parameter combinations are related to the location of the periodic orbits (mean firing rate), and the duration in which the system stays in the LPR mode.

Table 4-1: A slice-by-slice summary of FF statistical comparison between the *in vitro* hippocampal slice data and the CRG model output is shown. The model was able to match each seizure state with $P > 0.05$. The relative system excitability measure (k/β) is at its highest value during the ictal state.

Slice	Seizure State	β	K	X	P-value	k/β
1	Preictal	5	20	3	0.87	4.0
	Ictal	3	20	3	0.07	6.7
	Postictal	6	20	3	0.15	3.3
2	Preictal	6	10	3	0.27	1.7
	Ictal	3	20	3	0.47	6.7
	Postictal	4	10	2	0.08	2.5
3	Preictal	5	30	4	0.08	6.0
	Ictal	2	30	4	0.12	15.0
	Postictal	9	30	4	0.26	3.3
4	Preictal	3	20	3	0.10	6.7
	Ictal	1	10	3	0.13	10.0
	Postictal	3	20	3	0.84	6.7

4.3 Network State Space Analysis

Quantitative analysis on the nonlinear dynamics of the model output was performed. The Jacobian (J) of a single unit second order system (u_{1n} u_{2n}) that is isolated from the rest of the network was analyzed first before investigating the coupled network dynamics.

$$J = w_n \begin{bmatrix} V(x) - 3u_{1n}^2 - u_{2n}^2 & 1 + S_{\phi,n} - 2u_{1n}u_{2n} \\ -1 - S_{\phi,n} - 2u_{1n}u_{2n} & V(x) - 3u_{2n}^2 - u_{1n}^2 \end{bmatrix}. \quad \text{Eq. 4-1}$$

Solving the eigenvalues of Eq. 4-1 would give

$$\xi_{1,2} = w_n(V(x) \pm j(1 + S_{\phi,n})). \quad \text{Eq. 4-2}$$

The threshold function $V(x)$ would have a constant value of 1 for oscillators, resulting in an unstable focus at (0, 0). In the case of a threshold-based unit where $V(x)=0$, Hopf-bifurcation occurs and the (0, 0) becomes a stable focus.

By adjusting the β parameter alone while keeping the other model parameters identical, the transitions between interictal, preictal, ictal, and postictal dynamics can be created. An illustrative state space (u_{11} , u_{31} , u_{41}) for Unit One of a four-cell CRG model simulated data that best fit a low-Mg²⁺ *in vitro* model (using parameters from Table 2) is shown in Figure 4-4. The equilibrium points in model Unit One while the network exhibits high-complexity interictal state dynamics were found using Newton's method (a method for finding the approximate roots). In a projected state space of (u_{11} , u_{31} , u_{41}), the locations for some of these points can be found at (-0.278, -0.326, 0.642), (0.085, -0.259, 0.433), (0.293, -0.418, 0.892), and (0.179, -0.312, 1.172). In all these cases, the u_{31} state variable is negative in value.

These equilibrium points are saddle foci, as observed visually as well as from the calculation of the eigenvalues. The eigenvalues of the 16-by-16 Jacobian matrix were

obtained using MATLAB (R2007b). They consist of a mixture of real and complex values. The real parts of the eigenvalues indicate the stability of the manifolds, with positive values denoting instability and negative values denoting stability. The most positive (ξ_u) and negative (ξ_s) real parts for each of the identified equilibrium points were found to be ($\xi_u = 3.721 \pm 0.269$), and ($|\xi_s| = 4.474 \pm 0.002$) that correspond to the unstable and stable manifolds, respectively.

The changes from interictal to ictal states involved the escape from the saddle point foci in the state space trajectory. The preictal dynamics, transiting between interictal to ictal activity, does not appear to follow a direct path before settling on a more defined and quasi-periodic trajectory of the ictal state.

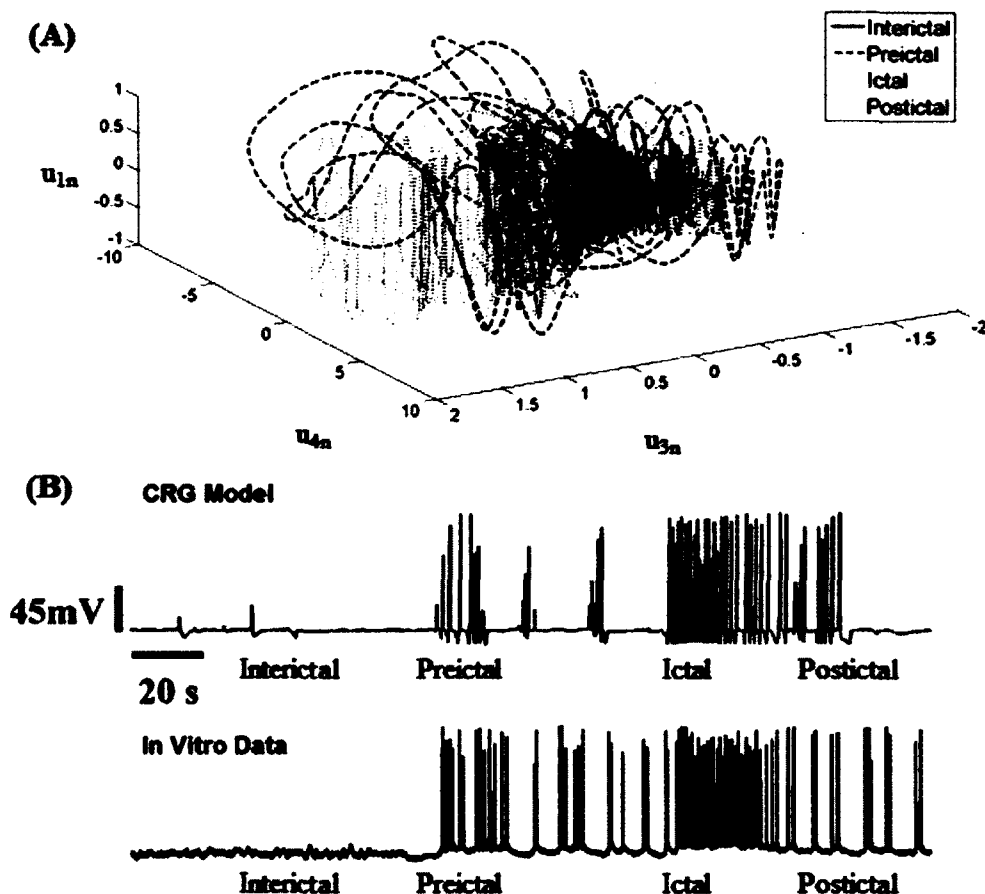


Figure 4-4: An illustrative example of the best-fit simulated CRG matched with the biological data is shown. (A) The state-space trajectories (u_{11} , u_{31} , u_{41}) for different β values in the simulation are shown, demonstrating that the onset of SLE can be visualized as the departure from the saddle point foci in interictal dynamics. The ictal dynamics exhibits a quasi-periodic trajectory. (B) The simulated signals (from Unit One of the model) along with the *in vitro* data (from Slice One) at different SLE states are also illustrated to show the similarity between the model output and the *in vitro* patch-clamp recordings. However, the similarity of the amplitude and the spike distribution still can be improved by adjusting the model parameters.

4.4 Negative Control Experiment

The negative control experiments were performed using the Mg-free solution on the rat hippocampal slice preparation, consisted of over six hours from three animals. Recurrent seizure-like activities (as shown in Figure 4-5) can be seen throughout. A total of 100 SLEs was observed. On average, the SLEs occurred eight to ten times every ten minutes and each SLE lasted half to two minutes.

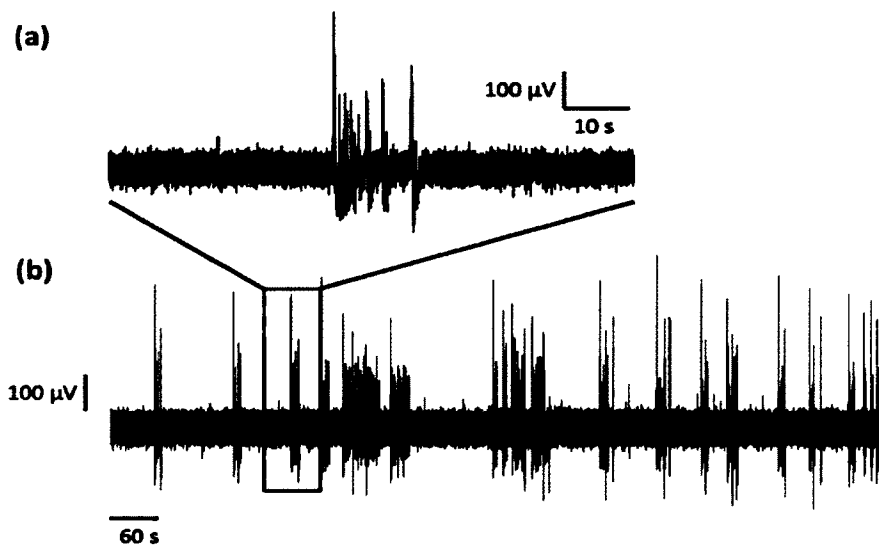


Figure 4-5: Sample field measurement from the negative control experiment showing repeated SLEs at approximately 8.30 ± 2.23 times every ten minutes.

4.5 Suppression of Seizure-Like Events

Once the NC trials have been completed, over five hours of PS and BP was performed under identical experimental condition. Two different stimulations were applied to the recording electrode when the ictal onset was detected. In most cases, the subsequent SLEs after a PS were delayed by over a minute while there was no obvious response with BP stimulation. Occasionally, a long period of interictal spiking activity would appear after PS. In these cases, the inter-seizure time was increased significantly. As an illustrative example in Figure 4-6, after a 15-second postictal stimulation, the subsequent SLE was prolonged for over six minutes and before resuming again. A ranksum statistic was performed using Matlab to compare the medians of the inter-seizure time between the NC, PS and the BP trials (Figure 4-7). The mean inter SLEs time of NC, PS and BP tests is 1 ± 0.56 min, 3.01 ± 2.07 min, and 0.82 ± 0.63 min. The SLEs were found to occur more frequently in the NC situation than with PS ($p < 0.002$). In the contrast experiment, the responses of NC situation and BP stimulation were similar ($p > 0.45$). Compared to PS stimulation, BP stimulation did not reduce the SLEs frequency ($p < 0.01$).

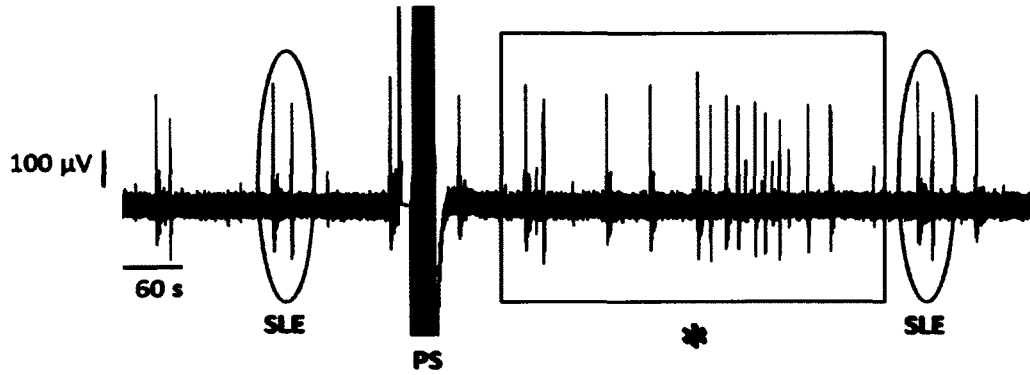


Figure 4-6: The effect of postictal stimulation (PS) on Mg-free in vitro hippocampal slice seizure model is shown. The seizure-like events are denoted as SLE. After stimulation (PS), interictal spiking events (*) were generated, leading to delayed or prolonged inter-seizure time.

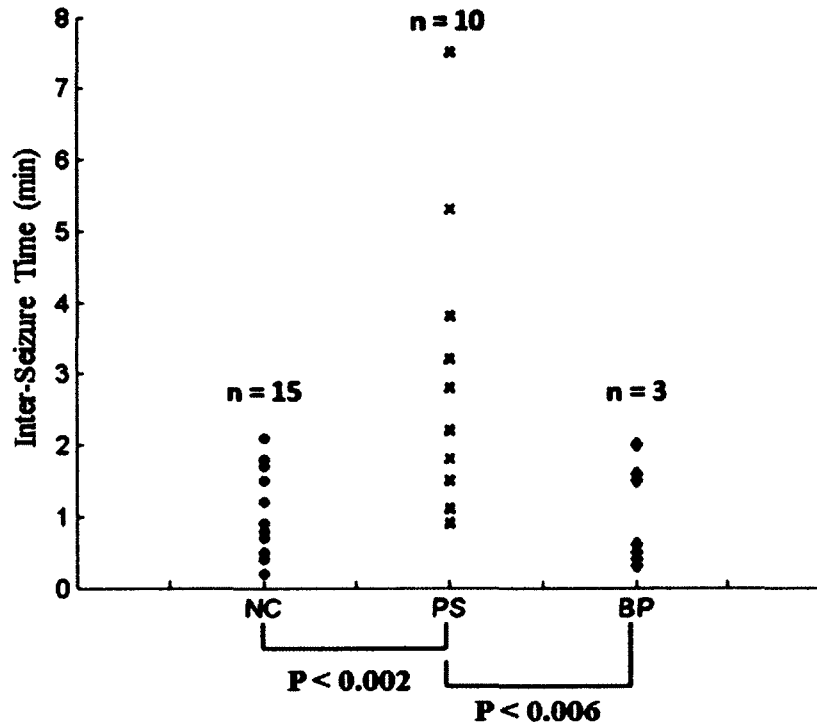


Figure 4-7: Ranksum statistics was performed on the negative control (NC) and postictal stimulation (PS) trials, showing that PS stimulation can prolong the inter-seizure time ($p < 0.002$).

CHAPTER 5

DISCUSSION

This chapter discusses the computational model in detail and describes the advantages and disadvantages of this modified new model. It also discusses the limitation of the seizure control strategy and the potential significance for seizure control therapy.

5.1 Slice Seizure Modeling

Neural oscillatory phenomena have been observed in many regions of the brain such as the cortex, the spinal cord and the soma of a primary afferent neuron (Compte et al., 2008; Pedroarena et al., 1999; Ruscheweyh & Sandkühler, 2005). Different patterns of seizure-like oscillations can be generated *in vitro* using various conditions as low-Mg²⁺, 4-AP, high-Ca²⁺ and other techniques (Gutiérrez et al., 1999; Luhmann et al., 2000; Li et al., 2008). The importance to the proposed modification lies in the versatility. It adds to the model unit to adapt to behaviors such as endogenous oscillation and threshold-based spiking with changes in a few model parameters (Zariffa & Bardakjian, 2006). The $V(x)$ parameter in this model controls whether a unit is an endogenous persistent oscillator or a threshold-based oscillator, depending on the type of neuron in the network. In addition to controlling the excitability, the kernel duration parameter β can also modulate the number of AP spikes in the threshold-based mode. Through the combination of endogenous oscillator units and threshold-based activation, a four-unit modified CRG model can

describe the dynamics of state transitions leading to seizure onsets in low-Mg²⁺ *in vitro* rat hippocampal model. The computer model can generate not only spontaneous seizures, but also induce slow biological state transitions. There are other plausible mechanisms underlying the observed non-spontaneous state transitions. Both intrinsic and extrinsic factors may lead to the modification of neuronal excitability over time. Some of the intrinsic factors include the type, number and distribution of the channel, the biochemical modification of the receptors, the activation of second-messenger systems, or even the modulating gene expression. Some examples of possible extrinsic factors include changes in ion concentration, alteration of synaptic contacts, long term potentiation, and modulating transmitter metabolism by glial cells. It has been suggested that system property changes lead to biological state transitions and that seizures may emerge because of a change in system parameters that may be invisible to passive observation (Richardson & Lopes da Silva, 2011).

The overall coupled network dynamics can also be attributed to the balance between the inhibitory feedback connection strengths and the kernel excitability. In general, the excitation parameters β and k have opposite effects on the LPR mode dynamics. Keeping the inhibitory feedback coefficients at a constant level, the kernel duration parameter has been found to be more sensitive than the modulation gain parameter to the changes in the overall kernel spectral energy. Excitability is related to the area under the kernel function and is estimated to be proportional to k/β . Even though the kernel duration is not related to the synaptic memory of the individual cells, the features related to the LPR dynamics were positively correlated to the ratio of the

modulation gain and first-order kernel duration (Figure 4-1). During the ictal period, the value of this ratio was also maximized.

The histogram representation of the ISI information was used as an initial analysis to obtain a small subset of CRG model parameter combinations that could match the whole-cell patch clamp recordings of CA3 pyramidal neurons undergoing state transitions to the ictal events. Then, the Fasano-Franceschini statistical method was applied to find the best model parameter combinations at different stages of SLE transitions. It has been observed that transitions from HPC interictal to LPR ictal state can be achieved by modulating the network excitability (Table 4-1).

Some short lasting state transitions can occur without external stimulation between the interictal and ictal regions of the model state space (Figure 4-4). This effect is consistent with previous reports and can be attributed to the finding that unstable periodic orbits can be embedded within chaotic manifolds (So et al., 1997). The major differences between the different parameter combinations are the location of the periodic orbits, the duration, and the interval in which the system stays in the LPR mode. The main findings presented here are consistent with previous results of Zalay et al. 2010, especially in regard to the relationship of β (kernel duration) to excitability and SLE properties. Furthermore, changes from interictal to ictal states involved the escape from the saddle point foci in the state space trajectory was also displayed in both the original (Zalay et al., 2010) and the modified version, except that the deviation in the state space trajectory in this case was induced by changes in model excitation parameters. Local stability analysis using Jacobian matrices around the equilibrium points uncovers the most unstable and stable manifolds around these points, leading to the discovery of

saddle point dynamics. Small negative u_{3n} state variables are always found to be in these interictal saddle points, where ictal episodes are typically associated with large swings in excitation level related to the magnitude of the mode response amplitude u_{3n} , (Zalay et al., 2010).

Despite the advantage of the modified CRG model in the elucidation of the system level mechanisms in modulating the network dynamics, traditional approaches such as conductance-based models are more suitable for the investigation of specific molecular properties of individual neuronal units. The proposed model also does not have a formal method to account for synaptic plasticity for long term simulation. Future work to improve this model includes the development of plasticity rules to enhance non-stationarity status and complexity of the model, thus narrowing the difference between the model and the physiological system behavior (Chiu et al., 2011).

Spontaneous SLEs have been generated by many different types of computational models. One must take into consideration that not all epilepsy disorders are the same. Epilepsy can occur in many different regions of the brain and each has its own unique characteristics. A slice-by-slice model must be created to enable customized stimulation protocol for each subject. The CRG model consists of external input portals for the simulation of current injection as well as electric field stimulation, which enables the evaluation of different stimulation protocols for the suppression and prevention of ictal activities. A previous simulation study has shown that biologically-inspired interictal signal is superior to other random or periodic stimulation protocols in the suppression of potential ictal events (Colic et al., 2011). The ability to quickly and effectively adjust the model parameters related to network excitability for individual subjects would have

significant implications on the development of this model-based interictal dynamic stimulation strategy. The significance of this work is that the interictal, preictal and postictal stages of epileptiform activity can be modeled utilizing one set of equations by varying the excitability parameters accordingly. This capability has implications for modeling and testing the controllability of the seizures. The idea of abolishing seizures via electrical stimulation is to attempt to reset the seizure neurons (Good et al., 2009), related to two possible factors: (1) The effective strength of the synaptic kernel x to the unit, related to β , which was studied in this manuscript. (2) The threshold of triggering action potentials, v_3 parameter in the function $V(x)$, which was fixed in this paper, but may be a variable for future studies.

5.2 Slice Seizure-Like Activity Control

Electrical signal stimulation is an effective method for controlling or suppressing seizure-like activities. Different types of electrical stimuli were found to act on the animal slices. These signals either elicited or reduced the seizure-like activity, which means the animal brains not only receive electrical signals but also recognize the signal pattern. It is not clear how to access the brain signal without disturbing or causing damage to the original neural system. A pattern carrying the wrong information perhaps induces seizure activity more strongly. Therefore, the stimulus design is a difficult challenge to this SLE control research.

In this dissertation a new type of stimulus called the computational seizure model based stimulus is introduced for controlling the SLEs. The idea is to obtain a seizure suppression pattern directly from the *in vitro* signal of the animal brain slices. The previous researches have proved that both low frequency stimulation (LFS) and high

frequency stimulation (HFS) are delivered for the suppression of the SLEs in the animal brain slices. The LFS means the stimulating signal has the frequency of 0.5, 0.75, 1, 2, 10, and 25 Hz. The stimulus with the frequency of 130 and 200 Hz is set for the HFS. Both the HFS and LFS can suppress within the certain time (Albensi et al., 2008; Khosravani et al., 2003; Good et al., 2009; Wyckhuys et al., 2010). Later researchers found that even a signal with 60 Hz frequency can block SLE with a longer time (Rajdev et al., 2011). In this case, the frequency of the stimulus may not play an important role in the seizure control strategy. According to this clue, people accomplished their research on other stimulus parameters including the pulse width, pulse amplitude and signal strength/duration. The results show that no single parameter can completely achieve abortion of the SLEs (Rajdev et al., 2011), which means we need a specific pattern for seizure stimulation strategy.

There is a potential pathway to obtain the desired pattern from animal brain activity itself. In the inside environment of the mature body, they exit the self-regulation function. When the seizure happens, the brain may send out the signal and try to recover this abnormal situation. Hence, to apply this type of signal that is similar with the animal's own brain signal could be the most effective way to investigate the neural system. There are two special findings that are closely related to the neural self-regulation function and the seizure recovery signal. First, synaptic input is able to tune the neuronal response. The synaptic current can independently tune the mean firing rate and variability while the synaptic conductance offer the strong ability of tuning the spike rate, variability and reliability (Dorval II et al., 2006). Second, the study of interneurons and pyramidal cells during the *in vitro* SLEs suggested that the correlations of their excitatory and

inhibitory spikes increased at the end of the SLEs (Ziburkus et al., 2006), which means that inside the neuronal network a spiking communication mechanism stops the SLEs. This spiking information is the signal pattern we want to abstract from the brain activity for the seizure suppression. Corresponding to the above, *in vitro* postictal signal can be the best choice for seizure stimulation. However, the postictal signal recorded from the animal slices contains much random noise which is difficult to remove. This random component of the postictal signal has the probability to elicit other SLEs that are not supposed to happen.

With the disadvantage of the *in vitro* postictal signal, we decided to use the postictal signal from our modified CRG seizure model. Researchers in the original CRG modeling group have selected the inter seizure signal from their model and injected it to their computational seizure model. The seizure-like activity was significantly reduced according to the model output after the stimulation (Colic et al., 2011). If the model output is sufficiently similar to the *in vitro* signal, it should work and be more convenient to stimulus control and seizure stimulation application. Therefore, in this dissertation the postictal signal is applied to the *in vitro* slice seizure model. Compared to the interictal signal, the postictal signal should contain more information about suppressing seizure because the interical signal may generate another ictal activity (SLE) later.

Oscillator-based stimulation protocol was tested for its effectiveness to suppress seizure episodes in an *in vitro* hippocampal slice preparation. The Mg-free setup was chosen because it was able to generate a high volume of recurrent seizure-like activities (Swartzwelder et al., 1987), which makes it a valuable model to evaluate our postictal stimulation protocol. The suppression of SLEs should not be to block the interseizure-

like discharges (Smith & Swann, 1986). During the experiment we found the potassium concentration must be very accurate; otherwise, the signal may show the interseizure-like activity which leads to inconsistent SLE. The accurate potassium concentration (3.3 mM) and the right temperature (31-33.5 °C) help to guarantee a longer time limitation of producing the repeat identified SLEs. This *in vitro* seizure model is very strict to the ion concentrations and temperature for getting the right SLEs. The recurrent seizure-like activities are excellent for testing all kinds of seizure stimulus on the animal slices, since it is easy to identify the preictal, ictal and postictal states from the SLE pattern.

After the PS stimulation, most subsequent SLEs were delayed by approximately one minute. In a few instances (about 20% of the time), long interictal spiking activity would appear after PS, which would significantly prolong the onset of the next SLE. The manifestation of the interictal spikes after postictal stimulation can be considered a temporary resetting of the slice and then the magnesium-free environment would induce seizure-like activities again. Meanwhile, there is no effective response from the bipolar pulse signal stimulation. Even in some cases it seems to increase the seizure activity (Figure 4-7). But some of the interictal time also reduced in the bipolar pulse signal stimulation comparing to the control experiment. Along with the stimulation results, the postictal signals did prolong the inter SLE time, which means they have a large chance to supply the spiking information of stopping SLEs.

The three postictal stimuli are selected from the modified CRG model with the parameter combination which can generate most common SLE patterns. They are randomly picked from the seizure-like field activity simulation and used as an example to test our computational seizure model-based stimulus. More tests with different

stimulating patterns under the altered strength need to be carried out to determine which stimuli will lead to seizure control or neuron resetting. One approach is to impose a baseline/control stimulus initially and then systematically vary the main stimulus features such as the spiking pattern, the amplitude, and the stimulation time. The electrical signals from the brain, as obtained from the simulation, would then be analyzed to generate rules that relate the stimulus characteristics to the brain signal.

In the modified CRG model, different parameter combinations that offer seizure patterns need to be considered. Seizure patterns can differ from individual to individual and from species to species. It is possible to match these patterns through changes in the CRG model input parameters. Those factors may enable the suppression of seizures through forced resetting of the neuronal network activities. However, the suppression was short-lived, before the next imminent SLE would start. At this stage, the postictal stimulus appeared to help reset the neuronal network into normal activity. However, more work is needed to evaluate the long term effect of such stimulation on the neurodynamics of the subjects.

This research may be applicable to the design of more effective deep brain stimulation strategies for epileptic patients. Selection of the resetting dynamics from the epileptic patient's own brain signal may enable a natural way to provide stimulation. If it is applied to the seizure disease in humans, the seizure lesion needs to be known before the stimulation. If a signal with unchanging characteristics is applied to the brain, nonstationary conditions within the lesion may cause that signal to be ineffective at some times or to even act as a trigger for the seizure. A more dynamic approach to stimulation may therefore be more safe and effective. In such an approach, the information from the

computational models for seizure prediction and stimulation would be stored in the stimulator and would be a component of a feedback loop in which the brain activity was measured and used to select the most appropriate stimulation.

CHAPTER 6

CONCLUSION AND FUTURE WORK

In this dissertation, we have presented a modified CRG model of transitions among preictal, ictal and postictal activity, which can fit into two various seizure patterns under different biological environments and provide a computational-based stimulus generating tool for seizure stimulation. This seizure model also can be applied to other types of seizure research. The original CRG model equations (oscillatory type) were modified into threshold-based CRG model equations to match the changes of seizure-like activity over time within the neuronal network. The biological data recorded by whole cell patch clamp techniques from the rat hippocampal slices was used to adjust to the model's parameter, which in turn offered different SLE patterns. After the biological data were incorporated into the modified CRG model, statistical comparisons were used to quantify the match between the biological data and model outputs. Network state space analysis was also performed to explain the seizure activity simulation orbits in three dimensions. Based on this identified computational seizure network model, we selected the postictal simulation signals as our stimuli to control SLE on the animal slice.

The signals from the model matched three states of the SLE over time. The changing curve of the parameter exhibit the inside process of the single SLE and the relationship among the excitation kernel, the mean firing rate and the number of SLEs. The

stimulation results demonstrated that postictal simulation signals could affect the SLE *in vitro*, which means that the model may be applicable for human seizure therapy.

Further research should focus on stimulus design for suppressing the SLEs and how to embed this stimulation strategy into the entire seizure control system. The specific factors related to the seizure control need to be discovered from the patterns of the stimulus. If possible, a common pattern that is effective for all types of SLEs should be sought. A final stage of this research would be to test the design of a deep brain stimulator (DBS) for human seizure therapy. In this case, a completed seizure feedback control system is required for the future test.

This seizure feedback control system (Figure 6-1) is to predict the seizure situation and reduce it beforehand. It consists of three functions: seizure prediction, seizure modeling, and seizure stimulation. We can induce different types of animal seizures or SLEs to test this negative control system. The prediction function is designed by the wavelet prediction system (WPS) with the accuracy above 90% (Chiu, 2006; Chiu, 2011). The stimulation is the output signal of CRG model that is going to inject postictal waveform to the neuron right before the seizure happens, which is to apply a small perturbation to the system and results that the action potentials stay away from the continuous seizure-like bursting. For example, after the seizure inducing solution is applied to the animal's brain slices, the WPS begins to work. The computational model based stimulator starts the signal injection every time when WPS have predicted the seizure. The WPS stops working after having predicted the seizure and be back to work after the stimulation has finished.

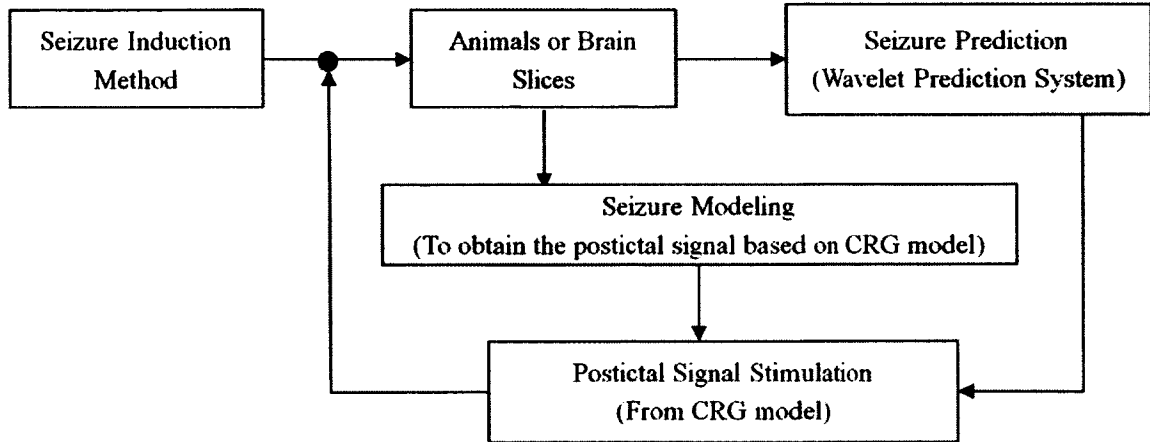


Figure 6-1: Sketch of the feedback control system for seizure suppression test.

This research may have potential implication in the therapy of epileptic patients, related to a better design for an adaptive deep brain stimulation strategy. Selecting the resetting dynamics from the epileptic patient's own brain signal is a possible way to enable a more natural way to provide stimulation.

APPENDIX A

THE MATLAB SOURCE CODE OF CRG MODEL

A.1 Main Function Code

```
clear all

close all

A = 0.75;

for B = 1 : 1 : 20

    for K = 10 : 10 : 20

clear actual_y

clear v

%% Number of units and intrinsic waveforms to use

warning off;

N = 4; % N is the number of oscillators in the network.

load Wfull.mat;

% Load the intrinsic waveform for CRG (Other options are W6 and W7 depending on
where the peak is located.

% There should be N number of such waveforms

% After loading this W.mat file, there is a Wfunction variable (membrane
% potential) and Wfreq (phase in rad).

% Modified so that it now has 30000 samples within 1 period!

% also this waveform should have been normalized by the RMS.

% Also note that Wfunction is between 0 and 1 here to keep it consistent
% with the differential equation.

% Make new waveform a global variable so that sub-routines can call them up.

global Wfunction; % Wfunctions should be (1 by 30000) [in mV above baseline]
```

```
global Wfreq;

global LeN;

LeN = length(Wfunction);

%% Defining model parameters

% Angular frequency

w = 2*pi* [1.01; 0.99; 1.11; 1.09]/1.5; % w is the intrinsic angular frequency. Size = N x
1;

% Offset factor

C0 = [-0.2; -0.2; 0; 0]; % c0 is the constant offset

% Simulation duration

t_last = 180; % Simulation end time (typically 600s)

global SampleIntv;

global SampleFreq;

% Sampling frequency

SampleFreq = 512; % Simulation sampling frequency

SampleIntv = 1/SampleFreq; % Simulation sampling interval

time = 0:SampleIntv:t_last;

T = length(time);

%% External Input

% This is the part where we are supposed to replace the external field

% perturbation with different Poisson noise

% Pick one type of spike...

%load FieldSpike.mat;
```



```

%load IntraSpike.mat

%[Train1,spiketime]=inhomotrain(T,spike,SampleFreq,100,FFreq);

%[Train2,spiketime]=inhomotrain(T,spike,SampleFreq,100,5);

Sf_e = zeros(N,1)*ones(1,T); % Sf_e is phi external input. Size = N x T;

Sf_e = awgn(Sf_e,36.5);

%Sf_e(1,:) = Train1;

% When we are working on current injection, then we will modify this one

F_e = zeros(N,1)*ones(1,T); % F_e is synaptic external input.Size = N x T;

%F_e(1,:) = Wweight*Train1;%change to 3

%F_e(4,:) = -Train2;

%% Initial conditions for each unit

% Make sure the array has NxN number of elements

v = [ 1; 0.001; 0; 0; % First unit
      0.001; 1; 0; 0; % Second unit
      -1; 0.001; 0; 0; % Third unit...
      0.001; -1; 0; 0];

% Most recent state variables (or now initial conditions). Size = 4N x 1;

% v1 and v2 are Euclidean coordinates

% v3 and v4 corresponds to dynamic mode (0, 0)

k = ones(N,1)*K; % k is modulatory gain

% default values for k is 1 for Wfull and 15 for W10.

%% Coupling parameters

C = [ 0.5, 0.5, -A, -A;

```

```

    0.5, 0.5, -A, -A;
    0.3, 0.3, 0, 0;
    0.3, 0.3, 0, 0];

% Cf is phi coupling factor. Size = N x N;

beta = ones(N,1)*B;

% In paper beta = 20 is normal

% beta = 1 is excitable

%%

% initialize updated_t, updated_v

updated_t = [];

updated_v = [];

actual_t = SampleIntv:SampleIntv:t_last;

actual_y = [];

y = zeros(N,1); % y_last is a column array

[t,v] = ode23(@subcrg0701,[actual_t],v,[],Sf_e,F_e,C,w,C0,k,beta);

v = v';

for i = 1:N,

    index = 4*i-4; % index is the index of state variable, NOT neural unit (start with 1,
5, etc...)

    % W(i) = interpol(v(index),v(index+1),Wfunction,36000); % angle is between -pi
to pi

    % OR

    for j = 1:length(actual_t);

```

```

    angle(j) = atan2(v(index+2,j),v(index+1,j)+eps);
    if angle(j) <=0, angle(j) = angle(j) + 2*pi; end;
    W(i,j) = Wfunction(ceil(angle(j)*LeN/2/pi));
    actual_y(i,j) = C0(i) + v(index+3,j) +
((sqrt(v(index+1,j)^2+v(index+2,j)^2))^20).*W(i,j);
    end;
end;
f = figure;
% title(['MCRG20110908 - a' num2str(A) 'b' num2str(B) 'k' num2str(K) 'w1.5Kr8X2'],
'fontsize', 12);
for i = 1:N,
    subplot(N,1,i);
    plot(actual_t,actual_y(i,:));
    ylabel(['Unit ', num2str(i), ' Output']);
    ylim([-10 110]);
    xlabel('Time (s)');
end;
% saveas(g, ['Network20101105Wavea' num2str(A) 'b' num2str(B) '.fig']);
% saveas(g, ['Network20101105Wavea' num2str(A) 'b' num2str(B) '.tif'], 'tif');
%f = figure;
[ISI, Peaks] = ThresDet(actual_y, SampleFreq, 15, 3, 1);
save(['MCRG20110908_a' num2str(A) 'b' num2str(B) 'k' num2str(K) 'w1.5Kr8X2' '.mat'],
'actual_t', 'actual_y', 'v', 'ISI', 'Peaks');

```

```
% saveas(f, ['Network20101105ISla' num2str(A) 'b' num2str(B) '.fig']);  
  
saveas(f, ['MCRG20110908_a' num2str(A) 'b' num2str(B) 'k' num2str(K) 'w1.5Kr8X2'  
'tif'], 'tif');  
  
end  
  
end
```

A.2 The Derivative Function of CRG Model

```

function dvdt = subcrg0701(t,v,Sf_e,F_e,C,w,C0,k,beta),

% Sub-routine for CRG

%

% Inputs...

%

% t = sub-interval to be analyzed.

% v = initial values of state for sub-interval = v_last. Size = 2*N x 1;

% Sf_e = external stimuli for phi portal. Size = N x T;

% F_e = external stimuli for synaptic ODE. Size = N x T;

% C = phi coupling factor. Size = N x N;

% w = intrinsic angular frequency of oscillator or labile. Size = N x 1;

% C0 = resting potential. Size = N x 1;

% k = modulatory gain. Size = N x 1;

% beta = mode decay constant. Size = N x 1;

global Wfunction;

global SampleFreq;

global LeN;

N = length(v)/4;

dvdt = zeros(4*N,1); % Make sure that dvdt same size as v. Size = 4N x 1;

y = zeros(N,1);

current = ceil(t*SampleFreq);

```

```

for i = 1:N,
    index = 4*i-4; % index is the index of state variable, NOT neural unit (start with 1, 5,
etc...)
    % W(i) = interpol(v(index),v(index+1),Wfunction,36000); % angle is between -pi to
pi
    % OR
    angle = atan2(v(index+2),v(index+1)+eps);
    if angle <=0, angle = angle + 2*pi; end;
    W(i) = Wfunction(ceil(angle*LeN/2/pi));
    y(i) = C0(i) + v(index+3)+(sqrt(v(index+1)^2+v(index+2)^2)).*W(i);
end;
Fn = C*y + F_e(:,current);
%%
for i = 1:N,
    index = 4*i-4;
    Ka = 10; % Net contribution of alpha portal to hourglass and labile
    Sa = [0 0 0 0];
    Kr = 8; % Net contribution of rho portal to hourglass and labile clock
    % X = [3 3 3 3];
    X = [2 2 2 2];
    % X = [4 4 4 4];
    x(i) = Ka.*Sa(i) + Kr* v(index+3)+X(i);
    % x = [100 1 100 2];

```

```

% v(3:4:15); % x is the driving
% stimulus (for hourglass and labile clock). Here Sr_hist is updated to
% the initial time of this sampling period only. Size = N x 1;
% v1, v2 and v3 are parameters for the threshold functions in labile clock.
v1 = 1; % Magnitude parameter for labile clock (ON/OFF)
v2 = 30; % Slope parameter for labile clock
v3 = 0.5; % Input threshold to activate labile clock
V(i) = getV(x,v1,v2,v3);
end
%%
r1 = 1;
r2 = 0.3; % Refractoriness (fraction of the intrinsic period)
r3 = 8; % Sharpness of the refractoriness threshold
for i = 1:N, % index i is reserved for the oscillator index
    index = 4*i-4;
    R(i) = r1 / ((1+(2*pi*r2/angle)^r3)^(0.5));
% Refractory as function of phase for oscillator. Size = 1 x N;
end;
%%
for i = 1:N,
    index = 4*i-4; % index is the index of state variable, NOT neural unit (start with 1, 5,
etc...)
    Sf(i) = C0(i) + k(i)*v(index+3) + Sf_e(i,current);

```

```

% Sf(i) = 0;

dvdtd(index+1,1) = w(i)*(v(index+2)*(1+Sf(i)) + v(index+1)*(V(i)-v(index+1)^2-
v(index+2)^2));

dvdtd(index+2,1) = w(i)*(-v(index+1)*(1+Sf(i)) + v(index+2)*(V(i)-v(index+1)^2-
v(index+2)^2));

dvdtd(index+3,1) = v(index+4);

dvdtd(index+4,1) = beta(i)*Fn(i) - 2*beta(i)*v(index+4) - beta(i)^2*v(index+3);

end;

% v(index+3)

```


A.3 Threshold Detection Function of CRG model

```

function [ISI, Peaks] = ThresDet(Input, fs, threshold, Num0, MinWidth)

%%%%%%%%%%%%%%%%%%%%%%%%%%%%%%%%%%%%%%%%%%%%%%%%%%%%%%%%%%%%%%%%%%%%%%%%

% [ISI, Peaks] = ThresDet(Input, fs, threshold, Num0, MinWidth)

% Compute the ISI as a function of time

%

% ISI = gives interspike interval in units of seconds

% Peaks = gives time of peaks

% Input = [N by L] N number of sequence, L length of sequence

% fs = sampling frequency

% threshold = threshold value

% Num0 = min number of below thresholds points prior to peak

% MinWidth = min width (samples) of above threshold points to consider

% spike.

%%%%%%%%%%%%%%%%%%%%%%%%%%%%%%%%%%%%%%%%%%%%%%%%%%%%%%%%%%%%%%%%%%%%%%%%

[N, L] = size(Input);

decsn = Input > threshold;

tmplte = [zeros(1,Num0) ones(1,MinWidth)];

tmplen = Num0 + MinWidth;

for i = 1:N,

    Peaks{i} = [];

    counter = 1;

    for j = 1:L-tmplen,

```

```

if decsn(i,j:j+tmplen-1) == tmplt,
    Peaks{i}(counter) = j/fs;
    counter = counter+1;
    j = j + tmplen;
end;

end;

% subplot(2,2,i);

if ~isempty(Peaks{i})
    ISI{i} = diff(Peaks{i});
% plot(ISI{i}(1:length(ISI{i})-1),ISI{i}(2:length(ISI{i})), '.');
% axis([0 100 0 100]);
% title(['ISI for unit ' num2str(i)], 'fontsize', 14);
%% if t == 1
%% title(['ISI20100929(2.0Mg)' num2str(10*(t-1)) '~' num2str(10*t) 'min'],
'fontsize', 9);
%% else
%% title(['ISI20100929(0.25Mg)' num2str(10*(t-1)) '~' num2str(10*t) 'min'],
'fontsize', 9);
%% end

else
    continue;
end;

end;
end;

```

A.4 Gaussian Function and R Function of CRG Model

```
function gauss = Gaussian(phase, mag, spread, peak);  
gauss = mag/spread *exp(-(phase-peak).^2)/(2*spread.^2));
```

```
function V = getV(x,v1,v2,v3),  
% V = v1 ./ (1+exp(-v2*(x-v3)));  
if x >= v3,  
    V = 1;  
else V = 0;  
end
```

A.5 Matching Function for Model Outputs and Biological Data

```

clear all;

close all;

A = 0.75;

for B = 1 : 1 : 20

    for K = 10 : 10 : 20

data_EX = load('20100916_MP_0normal_10lowMg(0.25)_70wash.atf');

fid = fopen(['Overlapped_Area_0912.txt'],'at');

fprintf(fid,['\n' '20100913_MP_0normal_10lowMg(0.25)_40wash.atf &
MCRG20110908_a' num2str(A) 'b' num2str(B) 'k' num2str(K) 'w2Kr8X2' '.mat' '\n']);

fclose(fid);

% ISI

a = 1;

f = figure;

for s = 1 : 4

    actual_y = data_EX(a:299999*s,2);

    input = actual_y';

    subplot(2,2,s);

    [ISI Peaks] = ThresDet(input, 500,-40,3,1,s);

    a = 299999 * s;

end

saveas(f, ['ISI20100929_0.25Mg.tif'], 'tif');

% Histogram For Experimental Data

```

```

actual_y = data_EX(570000:690000,2);

input = actual_y';

[ISI Peaks] = ThresDet(input, 500,-40,3,1);

f = figure;

[N, X] = hist(ISI{1,1},0:0.3:10);

bar(X, N./sum(N), 1);

ylim([0 1]);

xlim([0 10]);

xlabel('Time(s)');

ylabel('Normalized Distribution');

title(['Histogram20100929(0.25Mg,3min)'], 'fontsize', 14);

saveas(f, ['ISI_Pre13_a' num2str(A) 'b' num2str(B) 'k' num2str(K) 'w2' '.tif'], 'tif');

% Histogram For CRG Model Output

A = 0.75;

for B = 1 : 10

B = 10;

data_MO = load(['MCRG20110908_a' num2str(A) 'b' num2str(B) 'k' num2str(K)

'w1.5Kr8X3' '.mat']);

f = figure;

M = zeros(4,34);

for i = 1 : 4

subplot(2,2,i);

[M(i,:), Y] = hist(data_MO.ISI{1,i},0:0.3:10);

```

```

bar(Y, M(i,:)./sum(M(i,:), 1);

ylim([0 1]);

xlim([0 10]);

xlabel('Time(s)');

ylabel('Normalized Distribution');

title(['Histogram(a0.75b2k20) Unit' num2str(i) '(0.25Mg,10min)'], 'fontsize', 14);

saveas(f, ['Histogram_a0.75b2k20_Unit' num2str(i) '.tif'], 'tif');

end

saveas(f, ['Histogram_a0.75b1.tif'], 'tif');

% Normalized Histogram Overlapped Area Calculation

x = N./sum(N);

t = 0:0.3:10;

a = length(t);

total = zeros(1,4);

S = zeros(1,a);

for i = 1 : 4

    p(i,:) = M(i,:)./sum(M(i,:),);

end

for i = 1 : 4

    for j = 1 : a

        if x(j) >= p(i,j)

            S(i,j) = p(i,j);

            total(i) = total(i) + S(i,j);

        end

    end

end

```

```

    else
        S(i,j) = x(j);
        total(i) = total(i) + S(i,j);
    end
end
end
end

f = figure;
for i = 1:4
    subplot(2,2,i)
    plot(t,x,'or',t, p(i,:), 'og', t, S(i,:));
    ylim([0 1]);
    xlim([0 10]);
    xlabel('Time(s)');
    ylabel('Normalized Distribution');
    title(['Normalized Histogram Overlapped Area Is ' num2str(total(i)*100) '%'], 'fontsize',
    9);
    % saveas(f, ['NormalizedDistribution_a0.75b2k20_Unit' num2str(i) '.tif'], 'tif');
end
saveas(f, ['NormalizedDistribution_a0.75b2k20_Unit' num2str(i) '.tif'], 'tif');

G = 0.8;
if total(1) > G || total(2) > G || total(3) > G || total(4) > G,
    fid = fopen(['Overlapped_Area_0912.txt'],'at');

```

```

fprintf(fid,['Overlapped_Area_a' num2str(A) 'b' num2str(B) 'k' num2str(K) 'Kr8X3' '\n'
'%0.2f  %0.2f  %0.2f  %0.2f\n'],total);

fclose(fid);

end

    end

    end

end

%%

clear all;

data_EX = load('20100916_MP_0normal_10lowMg(0.25)_70wash.atf');

actual_y = data_EX(570000:690000,2);

input = actual_y';

[ISI Peaks] = ThresDet(input, 500,-40,3,1);

[L R] = size(ISI{1});

matrix(1:R-1,1) = ISI{1}(1,1:R-1);

matrix(1:R-1,2) = ISI{1}(1,2:R);

save EX_Sz_16.txt matrix -ASCII;

% clear all;

C = 1;

for i = 3 : 4

    [L R] = size(ISI{i});

    matrix(1:R-1,C) = ISI{i}(1,1:R-1);

```



```
matrix(1:R-1,C+1) = ISI{i}(1,2:R);  
C = C + 2;  
end  
save Model_Post_16.txt matrix -ASCII;
```

APPENDIX B

THE R PROGRAM CODE OF STATISTICAL ANALYSIS

```

rm(list=ls(all=TRUE))

library(mixAK)

library(mvtnorm)

## Bivariate KS Test: 2 Sample

## SAMPLING INDEPENDENTLY/SEPARATELY from FUSED 2 samples to
calculate boot test stats

modldat=read.table("C:/Documents and Settings/User/My Documents/Charles
Modelling/Good Fit/Model_Post_16.txt", header=F)

exptdat=read.table("C:/Documents and Settings/User/My Documents/Charles
Modelling/Good Fit/EX_Post_16.txt", header=F)

exptdat=exptdat[!duplicated(exptdat[,2]),]
exptdat=exptdat[!duplicated(exptdat[,1]),]

#exptdat=unique(exptdat)

dim(exptdat)dim(modldat)

#####

#MATRIX ASSUMPTIONS

modim=dim(modldat)

exdim=dim(exptdat)

pval=matrix(0,nr=modim[2]/2)

tststatvalp=matrix(0,nr=modim[2]/2)

rr=matrix(0,nr=modim[2]/2)

#####

#OVERALL LOOP

```

```

system.time(
for(l in 1:(modim[2]/2)){
#MODEL DATA
dd= modldat[ , (2*l-1):(2*l)]
dd=dd[!duplicated(dd[,2]),] #####CHANGE/CHECK THIS ALL THE
TIME
dd=dd[!duplicated(dd[,1]),]
#dd=unique(dd)
x1=dd[,1]
x1=x1[x1>0]
y1=dd[,2]
y1=y1[y1>0]
dd=cbind(x1,y1)
#EXPTAL DATA
x2=exptdat[,1]
y2=exptdat[,2]
dd2=cbind(x2,y2)
#STACKING FOR CRIT VALUE CALC
dd3=rbind(dd,dd2)
#####
#
#P-VALUE METHOD

```

```
n1=length(x1)
n2=length(x2)
nsim=500
tstatboot=matrix(0,nr=nsim)
#BOOT TEST STATS
for(k in 1:nsim){
#SAMPLING FOR GROUP 1
ddb=dd3[sample(n1, replace=T),]
#ddb=dd[sample(n1, replace=T),]
x1b=ddb[,1]
y1b=ddb[,2]
#SAMPLING FOR GROUP 2
dd2b=dd3[sample(n2, replace=T),]
#dd2b=dd2[sample(n2, replace=T),]
x2b=dd2b[,1]
y2b=dd2b[,2]
#STACKING
x3b=c(x1b,x2b)
y3b=c(y1b,y2b)
#ESTIMATED COUNTS
Gr1=matrix(0,nr=(n1+n2),nc=4)
Gr2=matrix(0,nr=(n1+n2),nc=4)
for(i in 1:(n1+n2)){
```

```

#GROUP 1
Gr1[i,1]=sum( ifelse( x1b <=x3b[i], 1,0)*ifelse( y1b <= y3b[i], 1,0) )/n1
Gr1[i,2]=sum( ifelse( x1b >=x3b[i], 1,0)*ifelse( y1b <= y3b[i], 1,0) )/n1
Gr1[i,3]=sum( ifelse( x1b >=x3b[i], 1,0)*ifelse( y1b >= y3b[i], 1,0) )/n1
Gr1[i,4]=sum( ifelse( x1b <=x3b[i], 1,0)*ifelse( y1b >= y3b[i], 1,0) )/n1
#GROUP 2
Gr2[i,1]=sum( ifelse( x2b <=x3b[i], 1,0)*ifelse( y2b <= y3b[i], 1,0) )/n2
Gr2[i,2]=sum( ifelse( x2b >=x3b[i], 1,0)*ifelse( y2b <= y3b[i], 1,0) )/n2
Gr2[i,3]=sum( ifelse( x2b >=x3b[i], 1,0)*ifelse( y2b >= y3b[i], 1,0) )/n2
Gr2[i,4]=sum( ifelse( x2b <=x3b[i], 1,0)*ifelse( y2b >= y3b[i], 1,0) )/n2
}
tstatboot[k]=max(abs(Gr1-Gr2))
}
#OBSERVED TEST STATISTIC CALCULATION
#STACKING AS ONE SAMPLE
x3=c(x1,x2)
y3=c(y1,y2)
#ESTIMATED PROBYs
datH1=matrix(0,nr=(n1+n2),nc=4)
datH2=matrix(0,nr=(n1+n2),nc=4)
for(i in 1:(n1+n2) ){
datH1[i,1]=sum( ifelse( x1 <=x3[i], 1,0)*ifelse( y1 <= y3[i], 1,0) )/n1
datH1[i,2]=sum( ifelse( x1 >=x3[i], 1,0)*ifelse( y1 <= y3[i], 1,0) )/n1

```

```

datH1[i,3]=sum( ifelse( x1 >=x3[i], 1,0)*ifelse( y1 >= y3[i], 1,0) )/n1
datH1[i,4]=sum( ifelse( x1 <=x3[i], 1,0)*ifelse( y1 >= y3[i], 1,0) )/n1
#EXPERIMENTAL
datH2[i,1]=sum( ifelse( x2 <=x3[i], 1,0)*ifelse( y2 <= y3[i], 1,0) )/n2
datH2[i,2]=sum( ifelse( x2 >=x3[i], 1,0)*ifelse( y2 <= y3[i], 1,0) )/n2
datH2[i,3]=sum( ifelse( x2 >=x3[i], 1,0)*ifelse( y2 >= y3[i], 1,0) )/n2
datH2[i,4]=sum( ifelse( x2 <=x3[i], 1,0)*ifelse( y2 >= y3[i], 1,0) )/n2
}
tststatvalp[l]=max(abs(datH1-datH2))
#P-VALUE
pval[l]=sum(ifelse(tstatboot>tststatvalp[l], 1, 0))/nsim
rr[l]=max(tstatboot)-min(tstatboot)
}
) #SYSTEM TIME
pval
which(pval>0.05)
pval[pval>0.05]
max(rr)/nsim
summary(rr)
summary(tststatvalp)

```

BIBLIOGRAPHY

Albensi, B. C., Toupin, J. D., Oikawa, K., & Oliver, D. R. (2008, August 21). Controlled pulse delivery of electrical stimulation differentially reduces epileptiform activity in Mg²⁺-free-treated hippocampal slices. *Brain Research*, 1226, 163-172.

Albrecht, D., Rausche, G., & Heinemann, U. (1989). Reflections of low calcium epileptiform activity from area CA1 into dentate gyrus in the rat hippocampal slice. *Brain Research*, 773(1-2), 173-180.

Avoli, M. (2007). The epileptic hippocampus revisited: back to the future. *Epilepsy Currents American Epilepsy Society*, 7(4), 116-118.

Babloyantz, A., & Destexhe, A. (1986). Low-dimensional chaos in an instance of epilepsy. *Proceedings of the National Academy of Sciences of the United States of America*, 83(10), 3513-3517.

Bardakjian, B. L., & Diamant, N. E. (1994). A mapped clock oscillator model for transmembrane electrical rhythmic activity in excitable cells. *Journal of Theoretical Biology*, 166(3), 225-235.

Berger, T. W., Ahuja, A., Courellis, S. H., Deadwyler, S. a, Erinjippurath, G., Gerhardt, G. a, Gholmieh, G., et al. (2005). Restoring lost cognitive function. *IEEE Engineering in Medicine and Biology Magazine*, 24(5), 30-44.

Brijesh, R., & Ravindran, G. (2007). A Spiking neural network of the CA3 of the hippocampus can be a neural prosthesis for lost cognitive functions. *Conference proceedings*: 29th Annual International Conference of the IEEE Engineering in Medicine and Biology Society, 2007, 4755-8.

Brivanlou, I. H., Dantzker, J. L. M., Stevens, C. F., & Callaway, E. M. (2004). Topographic specificity of functional connections from hippocampal CA3 to CA1. *Proceedings of the National Academy of Sciences of the United States of America*, 101(8), 2560-5.

Buck, D., Baker, G. a, Jacoby, a, Smith, D. F., & Chadwick, D. W. (1997). Patients' experiences of injury as a result of epilepsy. *Epilepsia*, 38(4), 439-44.

- Chakravarthy, N., Sabesan, S., Iasemidis, L., & Tsakalis, K. (2007). Controlling synchronization in a neuron-level population model. *International Journal of Neural Systems*, 17(2), 123-38.
- Chakravarthy, N., Tsakalis, K., Sabesan, S., & Iasemidis, L. (2009). Homeostasis of brain dynamics in epilepsy: a feedback control systems perspective of seizures. *Annals of Biomedical Engineering*, 37(3), 565-85.
- Chiu, A. W., Derchansky, M., Cotic, M., Carlen, P. L., Turner, S. O., & Bardakjian, B. L. (2011). Wavelet-based Gaussian-mixture hidden Markov model for the detection of multistage seizure dynamics: A proof-of-concept study. *BioMedical Engineering Online*, 10(1), 29.
- Chiu, A. W. L., Jahromi, S. S., Khosravani, H., Carlen, P. L., & Bardakjian, B. L. (2006). The effects of high-frequency oscillations in hippocampal electrical activities on the classification of epileptiform events using artificial neural networks. *Journal of Neural Engineering*, 3(1), 9-20.
- Chiu, A. W. L., Kang, E. E., Derchansky, M., Carlen, P. L., & Bardakjian, B. L. (2006). Online prediction of onsets of seizure-like events in hippocampal neural networks using wavelet artificial neural networks. *Annals of Biomedical Engineering*, 34(2), 282-94.
- Chon, K. H., Holstein-Rathlou, N. H., Marsh, D. J., & Marmarelis, V. Z. (1998). Comparative nonlinear modeling of renal autoregulation in rats: Volterra approach versus artificial neural networks. *IEEE Transactions on Neural Networks*, 9(3), 430-5.
- Cockerell O.C. (1996). The Mortality of Epilepsy. *Curr Opin Neurol*, 9(2), 93-6.
- Colic, S., Zalay, O. C., & Bardakjian, B. L. (2011). Responsive Neuromodulators Based on Artificial Neural Networks Used To Control Seizure-Like Events in a Computational Model of Epilepsy. *International Journal of Neural Systems*, 21(05), 367.
- Colpan, M. E., Li, Y., Dwyer, J., & Mogul, D. J. (2007). Proportional feedback stimulation for seizure control in rats. *Epilepsia*, 48(8), 1594-603.
- Compte, A., Reig, R., Descalzo, V. F., Harvey, M. A., Puccini, G. D., & Sanchez-Vives, M. V. (2008). Spontaneous high-frequency (10-80 Hz) oscillations during up states in the cerebral cortex *in vitro*. *Journal of Neuroscience*, 28(51), 13828-13844.
- Courellis, S. H., Zanos, T. P., Hsiao, M. C., Hampson, R. E., Deadwyler, S. a, Marmarelis, V. Z., & Berger, T. W. (2006). Modeling hippocampal nonlinear dynamic transformations with principal dynamic modes. *Conference proceedings* □: 28th Annual International Conference of the IEEE Engineering in Medicine and Biology Society, 1, 2300-3.

- Derchansky, M., Shahar, E., Wennberg, R. A., Samoiloa, M., Jahromi, S. S., Abdelmalik, P. A., Zhang, L., et al. (2004). Model of frequent, recurrent, and spontaneous seizures in the intact mouse hippocampus. *Hippocampus*, *14*(8), 935-947.
- Dorval, A. D., & White, J. a. (2006). Synaptic input statistics tune the variability and reproducibility of neuronal responses. *Chaos*, *16*(2), 026105.
- Fasano, G., & Franceschini, A. (1987). A multidimensional version of the Kolmogorov-Smirnov test. *Monthly Notices of the Royal Astronomical Society*, *225*(1), 155–170.
- Fisher, R., Salanova, V., Witt, T., Worth, R., Henry, T., Gross, R., Oommen, K., et al. (2010). Electrical stimulation of the anterior nucleus of thalamus for treatment of refractory epilepsy. *Epilepsia*, *51*(5), 899-908.
- FitzHugh, R. (1961). Impulses and Physiological States in Theoretical Models of Nerve Membrane. *Biophysical Journal*, *1*(6), 445-466.
- Gerstner, W., & Kistler, W. M. (2002). Spiking Neuron Models. (W. Maass & B. C, Eds.) *Physical Review E - Statistical, Nonlinear and Soft Matter Physics*, *66*, 041903.
- Good, L. B., Sabesan, S., Marsh, S. T., Tsakalis, K., Treiman, D., & Iasemidis, L. (2009). Control of synchronization of brain dynamics leads to control of epileptic seizures in rodents. *International Journal of Neural Systems*, *19*(3), 173-196.
- Gutiérrez, R., Armand, V., Schuchmann, S., & Heinemann, U. (1999). Epileptiform activity induced by low Mg²⁺ in cultured rat hippocampal slices. *Brain Research*, *815*(2), 294-303.
- Hemond, P., Epstein, D., Boley, A., Migliore, M., Ascoli, G. a, & Jaffe, D. B. (2008). Distinct classes of pyramidal cells exhibit mutually exclusive firing patterns in hippocampal area CA3b. *Hippocampus*, *18*(4), 411-24.
- Hodgkin, A. L., Huxley, A. F., & Katz, B. (1952). Measurement of current-voltage relations in the membrane of the giant axon of *Loligo*. *The Journal of Physiology*, *116*(4), 424-448.
- Iasemidis, Leon D, Shiau, D.-S., Sackellares, J. C., Pardalos, P. M., & Prasad, A. (2004). Dynamical resetting of the human brain at epileptic seizures: application of nonlinear dynamics and global optimization techniques. *IEEE Transactions on Biomedical Engineering*, *51*(3), 493-506.
- Isomura, Y., Fujiwara-Tsukamoto, Y., & Takada, M. (2008). A network mechanism underlying hippocampal seizure-like synchronous oscillations. *Neuroscience Research*, *61*(3), 227-33.

Izhikevich, E M. (2003). Simple model of spiking neurons. *IEEE Transactions on Neural Networks*, 14(6), 1569-72.

Izhikevich, Eugene M. (2004). Which model to use for cortical spiking neurons. *IEEE Transactions on Neural Networks*, 15(5), 1063-70.

Kamali, A. W., Cockerell, O. C., & Butlar, P. (2004). CASE REPORT Aneurysms and epilepsy: an increasingly recognised cause. *Seizure*, 13, 40-44.

Kang, E. E., Zalay, O. C., Cotic, M., Carlen, P. L., & Bardakjian, B. L. (2010). Transformation of neuronal modes associated with low-Mg²⁺/high-K⁺ conditions in an in vitro model of epilepsy. *Journal of Biological Physics*, 36(1), 95-107.

Kasugai, M., Akaike, K., Imamura, S.-ichi, Matsukubo, H., Tojo, H., Nakamura, M., Tanaka, S., et al. (2007). Differences in two mice strains on kainic acid-induced amygdalar seizures. *Biochemical and Biophysical Research Communications*, 357(4), 1078-83.

Khosravani, H., Carlen, P. L., & Velazquez, J. L. P. (2003). The control of seizure-like activity in the rat hippocampal slice. *Biophysical Journal*, 84(1), 687-95.

Khosravani, H., Pinnegar, C. R., Mitchell, J. R., Bardakjian, B. L., Federico, P., & Carlen, P. L. (2005). Increased high-frequency oscillations precede in vitro low-Mg seizures. *Epilepsia*, 46(8), 1188-97.

Lapicque, L. (2007). Quantitative investigations of electrical nerve excitation treated as polarization. 1907. *Biological Cybernetics*, 97(5-6), 341-9.

Lehnertz, K., & Elger, C. (1998). Can Epileptic Seizures be Predicted? Evidence from Nonlinear Time Series Analysis of Brain Electrical Activity. *Physical Review Letters*, 80(22), 5019-5022.

Levy, W. B., Desmond, N. L., & Zhang, D. X. (1998). Perforant path activation modulates the induction of long-term potentiation of the schaffer collateral--hippocampal CA1 response: theoretical and experimental analyses. *Learning & Memory*, 4(6), 510-518.

Li, Y., Fleming, I. N., Colpan, M. E., & Mogul, D. J. (2008). Neuronal desynchronization as a trigger for seizure generation. *IEEE Transactions on Neural Systems and Rehabilitation Engineering*, 16(1), 62-73.

Luhmann, H. J., Dzhala, V. I., & Ben-Ari, Y. (2000). Generation and propagation of 4-AP-induced epileptiform activity in neonatal intact limbic structures in vitro. *The European Journal of Neuroscience*, 12(8), 2757-68.

Merlin, L. R. (2009). Making Generalizations about Seizure Propagation. *Epilepsy Currents*, 9(1), 24-25.

- Morrell, M. J. (2011). Responsive cortical stimulation for the treatment of medically intractable partial epilepsy. *Neurology*, 77(13), 1295-1304.
- Morris, C., & Lecar, H. (1981). Voltage oscillations in the barnacle giant muscle fiber. *Biophysical Journal*, 35(1), 193-213.
- Nagumo, J., Arimoto, S., & Yoshizawa, S. (1962). An Active Pulse Transmission Line Simulating Nerve Axon. *Proceedings of the IRE*, 50(10), 2061-2070.
- Nair, S. P., Shiau, D.-S., Principe, J. C., Iasemidis, L. D., Pardalos, P. M., Norman, W. M., Carney, P. R., et al. (2009). An investigation of EEG dynamics in an animal model of temporal lobe epilepsy using the maximum Lyapunov exponent. *Experimental Neurology*, 216(1), 115-121.
- Netoff, T. I., Clewley, R., Arno, S., Keck, T., & White, J. a. (2004). Epilepsy in small-world networks. *The Journal of Neuroscience*, 24(37), 8075-83.
- Pedroarena, C. M., Pose, I. E., Yamuy, J., Chase, M. H., & Morales, F. R. (1999). Oscillatory membrane potential activity in the soma of a primary afferent neuron. *Journal of Neurophysiology*, 82(3), 1465-1476.
- Rajdev, P., Ward, M., & Irazoqui, P. (2011). Effect of Stimulus Parameters in the Treatment of Seizures By Electrical Stimulation in the Kainate Animal Model. *International Journal of Neural Systems*, 21(02), 151.
- Richardson, M. P., & Lopes da Silva, F. H. (2011). TMS studies of preictal cortical excitability change. *Epilepsy Research*, 97(3), 273-277.
- Ruscheweyh, R., & Sandkühler, J. (2005). Long-range oscillatory Ca²⁺ waves in rat spinal dorsal horn. *European Journal of Neuroscience*, 22(8), 1967-1976.
- Schmidt, D., & Löscher, W. (2005). Drug resistance in epilepsy: putative neurobiologic and clinical mechanisms. *Epilepsia*, 46(6), 858-877.
- So, P., Ott, E., Sauer, T., Gluckman, B. J., Grebogi, C., & Schiff, S. J. (1997). Extracting unstable periodic orbits from chaotic time series data. *Physical Review E*, 55(5), 5398-5417.
- Stacey, W. C., & Litt, B. (2008). Technology insight: neuroengineering and epilepsy-designing devices for seizure control. *Neurology*, 4(4), 190-201.
- Su, Y., Radman, T., Vaynshteyn, J., Parra, L. C., & Bikson, M. (2008). Effects of high-frequency stimulation on epileptiform activity in vitro: ON/OFF control paradigm. *Epilepsia*, 49(9), 1586-93.

Swartzwelder, H. S., Lewis, D. V., Anderson, W. W., & Wilson, W. A. (1987). Seizure-like events in brain slices: suppression by interictal activity. *Brain Research*, 410(2), 362-366.

Traynelis, S. F., & Dingledine, R. (1988). Potassium-induced spontaneous electrographic seizures in the rat hippocampal slice. *Journal of Neurophysiology*, 59(1), 259-76.

Wagenaar, D. a, Madhavan, R., Pine, J., & Potter, S. M. (2005). Controlling bursting in cortical cultures with closed-loop multi-electrode stimulation. *Journal of Neuroscience*, 25(3), 680-8.

Walther, H., Lambert, J. D., Jones, R. S., Heinemann, U., & Hamon, B. (1986). Epileptiform activity in combined slices of the hippocampus, subiculum and entorhinal cortex during perfusion with low magnesium medium. *Neuroscience Letters*, 69(2), 156-61.

Wolf A, Swift JB, Swinney HL, Vastano JA. (1985). Determining Lyapunov exponents from a time series. *Physica D*, 16, 285–317.

Wyckhuys, T., Boon, P., Raedt, R., Van Nieuwenhuysse, B., Vonck, K., & Wadman, W. (2010). Suppression of hippocampal epileptic seizures in the kainate rat by Poisson distributed stimulation. *Epilepsia*, 51(11), 2297-304.

Yeckel, M. F., Kapur, a, & Johnston, D. (1999). Multiple forms of LTP in hippocampal CA3 neurons use a common postsynaptic mechanism. *Nature Neuroscience*, 2(7), 625-33.

Zalay, O. C., & Bardakjian, B. L. (2008). Mapped clock oscillators as ring devices and their application to neuronal electrical rhythms. *IEEE Transactions on Neural Systems and Rehabilitation Engineering*, 16(3), 233-44.

Zalay, O. C., Serletis, D., Carlen, P. L., & Bardakjian, B. L. (2010). System characterization of neuronal excitability in the hippocampus and its relevance to observed dynamics of spontaneous seizure-like transitions. *Journal of Neural Engineering*, 7(3), 036002.

Zariffa, J., & Bardakjian, B. L. (2006). Neuronal Electrical Rhythms Described by Composite Mapped Clock. *Annals of Biomedical Engineering*, 34(1), 128-141.

Zariffa, J., Ebdem, M., & Bardakjian, B. L. (2004). A synaptic input portal for a mapped clock oscillator model of neuronal electrical rhythmic activity. *Journal of Neural Engineering*, 1(3), 158-164.

Ziburkus, J., Cressman, J. R., Barreto, E., & Schiff, S. J. (2006). Interneuron and pyramidal cell interplay during in vitro seizure-like events. *Journal of Neurophysiology*, 95(6), 3948-54.

van Drongelen, W., Lee, H. C., Stevens, R. L., & Hereld, M. (2007). Propagation of Seizure-Like Activity in a Model of Neocortex. *Journal of Clinical Neurophysiology*, 24(2), 182-8.